Grain boundary diffusion during active pressure solution in NaCl:

Determination via resistivity and compaction experiments

Robert Farla (0124125)

BSc project submitted to the department of Earth Sciences, Utrecht University, 23-09-2004

Grain boundary diffusion during active pressure solution in NaCl:

Determination via resistivity and compaction experiments

Robert Farla

Abstract

Previous experiments have proven that pressure solution can indeed occur in granular salt at room temperature conditions and at fairly low stresses and that diffusion is the rate limiting process. However, at the microscopic scale the operating processes in the grain boundaries are still poorly understood because there are many unknown factors. It is also difficult to set up an experiment that takes into consideration all known factors, such as the geometry of grains, grain mineralogy, cementation, and solution chemistry in a grain boundary only up to 10 nanometres thick.

This investigation has two objectives. 1) To verify that pressure solution is diffusion controlled and occurs in both granular salt and at a halite crystal–glass contact for compaction experiments and an electrical resistivity experiment respectively. 2) To calculate Z* values for all experiments and compare them and determine which of the three factors, D, C, and S has the greatest influence on the rate limiting process, diffusion. Z* is the effective grain boundary diffusivity (m^3/s) and is written as Z* = DCS, where D is the solute diffusion coefficient in the grain boundary (m^2/s), C is the solubility of the diffusing species (m^3/m^3), and S is the average grain boundary fluid thickness, (m). The first set of experiments are one-dimensional compaction experiments performed on brine-saturated NaCl aggregates (grain size ~35 – 160 μm) at room temperature and with applied effective stresses in the range of 0.82 – 5.81 MPa. The other experiment is the measurement of resistivity in a single, annular halite-glass contact undergoing active pressure solution. The Z* values for the compaction experiments were calculated via a diffusion controlled strain rate equation and compaction displacement data whereas for the electrical resistivity experiment, Z* was calculated via the Nernst-Einstein equation and the resistivity measurements.

Results from the compaction experiments obey the micromechanical theory; $\dot{\varepsilon} \approx e_v^{-q} \cdot \sigma_e^n \cdot d^{-p}$ where e_v is the volumetric strain, σ_e, the effective stress, and d, the grain size and $q \approx 2$, n is slightly higher than 1, and $p = 3$ which proves that pressure solution in salt is diffusion dependent. The Z* values obtained lie in the range 3E-21 – 4E-19 m^3/s and show for a grain size of 35 μm first a positive dependence on the average normal stress (σ_n) and at σ_n greater than 10 MPa, the dependence becomes inversely proportional. For grain sizes greater than 85 μm, the relationship is only inversely proportional. Results from the electrical resistivity experiment yield Z* values in the range of 2E-20 – 2E-16 m^3/s with more data points towards the lower end and also shows an inverse dependence on σ_n. All results agree reasonably well with values from previous work on single contact and polycrystalline compaction experiments except for some Z* values in the electrical resistivity experiment at the upper end at 2E-16 m^3/s. In addition, variation in Z* in the results could indicate changes in S, but this cannot be said with certainty.

Contents

1. Introduction

This investigation on pressure solution in salt is carried out in order to find out more about the characteristics of this compaction process in nature, e.g. salt domes or gypsum flow allowing thrusting to occur. Past research and experiments have clearly demonstrated that sedimentary deposits in the presence of water and under substantial pressure may undergo a different compaction process than crystal plasticity for instance. Pressure solution, otherwise known as dissolution-precipitation creep is therefore an important mechanism of compaction in those materials, but also for the healing, sealing, and strength recovery in active fault zones [Hickman and Evans, 1992 , Bos and Spiers, 2000 , Bos et al., 2000 , Hickman and Evans, 1991 , Hickman and Evans, 1995 , Sleep and Blanpied, 1992]. Pressure solution in gypsum is also important for evaporate flow and understanding the processes involved with it [Spiers et al., 1990 , de Meer and Spiers, 1995].

Pressure solution in salt, often used as an analogue rock, has been extensively investigated in the past, but still many details of the exact processes that occur at the grain boundaries is unclear. Pressure solution is the dissolution, diffusion, and precipitation of salt from the grain boundaries to the pores in a granular material such as salt, gypsum, or sandstone or some other porous wetted aggregate under pressure. The word pressure is used and not stress because the watery solution in the pores of the material create a hydrostatic stress, meaning that stress can come from all directions. The grains are in random contact with each other. At that contact there is a normal stress which has been proven to be the key factor in pressure solution because at the grain-to-grain contacts dissolution occurs under the influence of normal stress acting on the boundaries of the grains. Pressure solution is further governed by time, grain size, d, temperature, T, applied stress, σ_e, porosity, ϕ and volumetric strain, e_v. The factor that relates these properties together is the volumetric strain rate, $\dot{\varepsilon}$. Other important factors include: geometry of grains, grain mineralogy, cementation, and solution chemistry and all counteract with each other making pressure solution a very complex compaction process to understand. Also the rate generally increases with increasing temperature or with effective pressure and with decreasing grain size [Yang, 1997].

Salt has proven to demonstrate pressure solution very well at room temperature and at relatively low stresses of 0.82 MPa to 7.4 MPa as used in this investigation for both the compaction experiments of granular salt and the electrical resistivity experiment on a salt crystal. In addition, the strain rates achieved are fast enough to record data in as much as 30 minutes (for the compaction experiments) unlike with any other materials such as quartz where the strain rate is so slow, it can take up to several weeks before substantial data is acquired. In addition, the behaviour of pressure solution in salt is relatively well understood from compaction, deformation, and single grain contact experiments. However, the internal structure, properties, and wettability of the grain boundaries are still hotly debated. Three models exist today about the nature of the grain contact boundary; 1) the thin fluid film model, 2) the dynamic island channel model [Tada and Siever, 1985], and 3) the microcrack model [den Brok and Spiers, 1991]. Fortunately for this investigation it is not important to know which model is 'correct'. Salt has been proven to be a good analogue specifically by den Brok et al. [den Brok et al., 1999]. They were investigating the possibility that salt could also be compressed by processes as crystal plasticity. They carried out the same experiments on NaCl as in this investigation and also on another material, $NaClO_3$, which is know to be a very soluble, elastic-brittle salt that cannot be deformed plastically at room pressure and temperature conditions. They found out that the relationship between $\dot{\varepsilon}$ and d, σ_e, e_v is strikingly similar for both materials [den Brok et al., 1999].

In order to prove that pressure solution is indeed happening with 'wetted' salt, various experiments were set up; compaction of granular salt under different starting conditions including constant applied stress or grain size and an electrical resistivity experiment for a salt crystal in contact

with a glass cone. Furthermore, from the results of these experiments, the diffusivity, Z* of salt in the grain boundaries of the salt grains and in the NaCl-glass contact will be found and compared. Both experiments were originally designed by Spiers, et al. [Spiers and Brzesowsky, 1993] and De Meer, et al. [de Meer et al., 2002] respectively. Other experiments have been designed for the same purpose by Spiers et al. [Schutjens and Spiers, 1999] and Hickman and Evans [Hickman and Evans, 1995], to quantify the diffusion coefficient, Z* for NaCl by means of using a salt crystal instead of granular salt samples for the reason that "the stress-induced convergence between crystals in quasi-saturated solution is probably better addressed in experiments on pairs of single crystals. There the displacement rate is not smoothed by averaging over a large number of independent interfaces between converging crystals, but is very small compared to that achieved in the compaction experiments" [Martin et al., 1999].

For the compaction experiments it was also useful to verify that pressure solution in granular salt with the presence of a brine solution is diffusion dependent, else there would be not much use in finding the diffusion coefficient, Z*. Much theory has already been addressed in previous work but for clarification purposes most of it has been addressed again in this paper in section II for both experiments.

For the electrical conductivity experiment, the Nernst-Einstein equation was used to relate the resistivity in the NaCl-glass contact to the diffusion of Na^+ and Cl^- ions in and out of the contact. Z*, also called the effective grain boundary diffusivity is actually equal to three other variables; Z* = DCS (m^3/s), where D is the solute diffusion coefficient in the grain boundary fluid (m^2/s), C is the solubility of the diffusing species (m^3/m^3), and S is the average grain boundary fluid thickness (m).

Because in previous experimental work it was unsure which of the three really controls Z*, the compaction experiments and the electrical resistivity experiment in this investigation are compared side by side in order to learn more about Z*.

2. Theoretical considerations

2.1. Derivation of the diffusion controlled strain rate equation for intergranular pressure solution (IPS) in the compaction experiments

The derivation of the strain rate equation for pressure solution in simple compaction experiments was originally discovered by Spiers, et al. [Spiers and Brzesowsky, 1993]. This derivation is slightly modified, however, assuming at first that the granular salt, which will be compressed, has no pore spaces, so no volumetric strain can occur. Standard symbol notation is used.

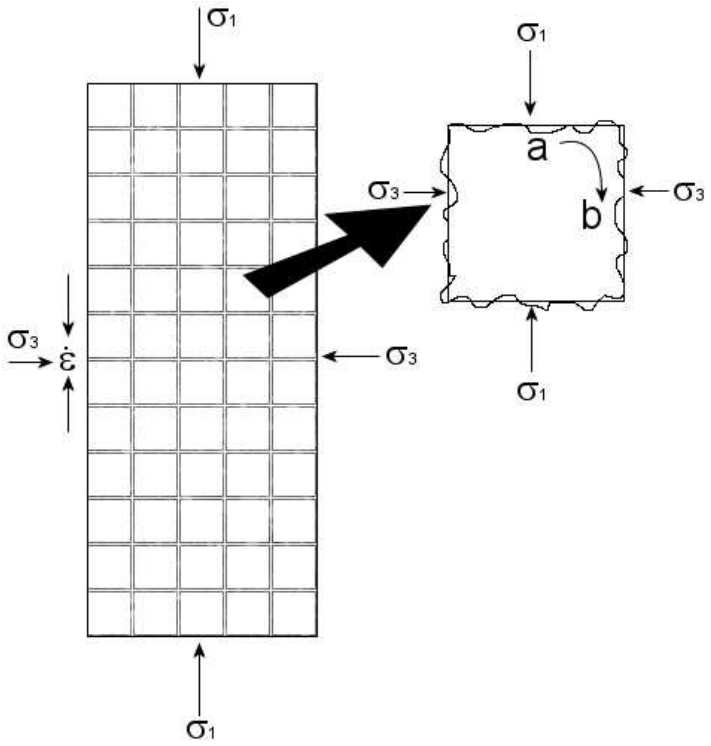

Image 1. A hypothetical column of salt grains under stress σ_1. One grain is taken out that illustrates the flux of atoms during pressure solution from a to b.

The chemical potential at 'a' is defined by:

$$\mu_a = f^s + \sigma_1 \Omega^s \tag{1.1}$$

Whereas the chemical potential at 'b' is defined by:

$$\mu_b = f^s + \sigma_3 \Omega^s \tag{1.2}$$

Where f^s is the Helmholtz free energy and Ω^s is the molar volume of the solid.

Then the potential difference from a => b is (1.1) subtracted from (1.2):

$$\Delta\mu = (\sigma_1 - \sigma_3)\Omega^s \tag{1.3}$$

This causes a difference in solubility ΔC. The solubility at 'a' is equal to:

$$\mu_a = \mu_0 + RT \ln\left(\frac{C_a}{C_0}\right) \tag{1.4}$$

And similarly at 'b':

$$\mu_b = \mu_0 + RT \ln\left(\frac{C_b}{C_0}\right) \tag{1.5}$$

Thus from a => b we get:

$$\Delta\mu = RT \ln\left(\frac{C_a}{C_b}\right) = (\sigma_1 - \sigma_3)\Omega^s \tag{1.6}$$

Because $C_a = C_b + \Delta C$ we can write Eq. 1.6 as:

$$RT\ln\left(\frac{C_b+\Delta C}{C_b}\right)=(\sigma_1-\sigma_3)\Omega^s$$

$$RT\ln\left(1+\frac{\Delta C}{C_b}\right)=(\sigma_1-\sigma_3)\Omega^s$$

$$1+\frac{\Delta C}{C_b}=\exp\left(\frac{(\sigma_1-\sigma_3)\Omega^s}{RT}\right)$$

$$\frac{\Delta C}{C_0}=\exp\left(\frac{(\sigma_1-\sigma_3)\Omega^s}{RT}\right)-1 \qquad (1.7)$$

This is the exact equation for the change in concentration divided by the original concentration. However, more than often it is that case that $\frac{\Delta C}{C_0} < 1$. If so, then the equation can be rewritten to an approximate equation:

$$\frac{\Delta C}{C_0}\approx\left(\frac{\sigma_1-\sigma_3}{RT}\right)\Omega^s \qquad (1.8)$$

Then next figure shows what happens to the flux of atoms also on a 1-D scale:

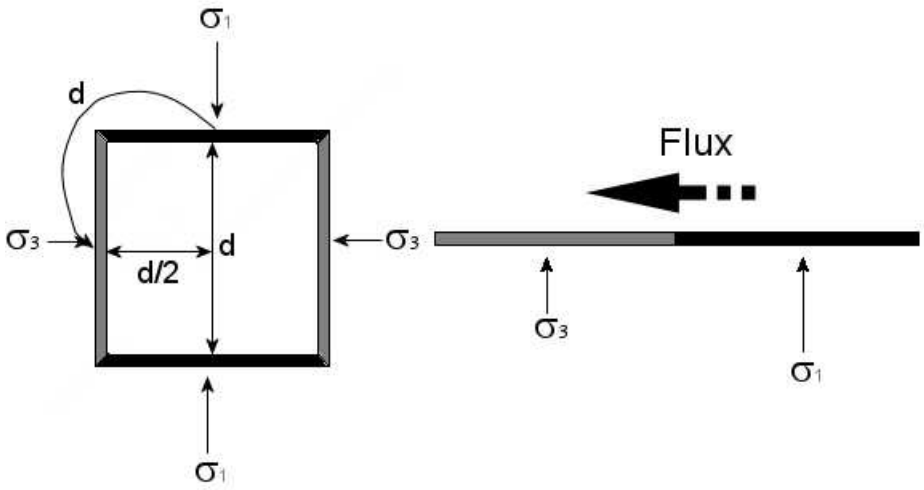

Image 2. The flux of atoms around a grain

The movement of a dissolved solid across a concentration gradient obeys Fick's law of diffusion shown below:

$$J=-D\frac{dC}{dx} \qquad (1.9)$$

The flux of atoms through a grain boundary liquid film is roughly equal to the following:

$$J \approx D\frac{\Delta C}{\Delta x} \tag{1.10}$$

Where J is the flux in mol/m^{2}s, D is the diffusion coefficient in m^2/s, C is the concentration in mol/m^3, and x is the distance in m. $\frac{dC}{dx}$ is the concentration gradient.

Figure 2 shows that $\Delta x \approx d$ where d is the grain size. Note that the diffusion coefficient is usually equal to $D = D_0 \exp\left(-\frac{Q}{k_B T}\right)$, where Q is the activation energy, k_B the Boltzmann constant, T is the temperature and D_0 is a pre-exponential factor (a constant).

With this the strain rate equation for diffusion controlled pressure solution can be derived for the first the approximate case and then the exact case.

Approximate case:

Substituting $\Delta x \approx d$ and Eq. 1.8 into Eq. 1.10 we get:

$$J = DC_0 \frac{\left(\frac{(\sigma_1 - \sigma_3)\Omega^s}{RT}\right)}{d} = DC_0 \frac{(\sigma_1 - \sigma_3)\Omega^s}{RTd} \tag{1.11}$$

Furthermore, the strain rate is equal to the extension per unit time divided by the original length:

$$\dot{\varepsilon} = \frac{\dot{l}}{l} \tag{1.12}$$

Where $l = \frac{d}{2}$ and $\dot{l}$ is equal to the volume flow per unit time divided by the area of the face of the grain. The volume flow per unit time = flux * area window * number of gradients, whereas the area of the face equals d^2.

$$\dot{l} = \frac{J \cdot w \cdot d \cdot 4}{d^2} \tag{1.13}$$

Substituting Eq. 1.13 into Eq. 1.12 we get:

$$\dot{\varepsilon} = \frac{J \cdot w \cdot d \cdot 4 \cdot 2}{d^3} = J\frac{8wd}{d^2} \tag{1.14}$$

Where w is the width of the fluid film between the grains where they come in contact.
Substituting Eq. 1.11 into Eq. 1.14 we get:

$$\dot{\varepsilon} = DC_0 w \frac{8(\sigma_1 - \sigma_3)\Omega^s}{RTd^3} \tag{1.15}$$

This can be rewritten with more familiar terminology as:

$$\dot{\varepsilon}_D = 8 \cdot DCS \frac{\sigma_e \Omega}{RTd^3} \tag{1.16}$$

Where w = S and $(\sigma_1 - \sigma_3) = \sigma_e$. Then lastly because it was assumed the medium was granular salt but without pore spaces, in actuality no strain could occur. Therefore the equation is slightly modified to account for pore spaces and volumetric strain:

$$\dot{\varepsilon}_D = A_D \cdot DCS \frac{\sigma_e \Omega}{RTd^3} \cdot \frac{1}{e_v^{2-4}} \tag{1.17}$$

Where 8 has been incorporated into the constant A_D and the three variable DCS equal Z*, the diffusivity constant.

Exact case

For the exact case the following is obtained. First Eq. 1.7 is substituted into Eq. 1.10 giving:

$$J = DC_0 \frac{\exp\left(\frac{\sigma_1 - \sigma_3}{RT}\Omega^s\right) - 1}{d} \tag{1.18}$$

Then substituting Eq. 1.18 into Eq. 1.14 gives:

$$\dot{\varepsilon}_D = 8DC_0 w \frac{\exp\left(\frac{\sigma_1 - \sigma_3}{RT}\Omega^s\right) - 1}{d^3}$$

$$\dot{\varepsilon}_D = A_D \cdot DCS \frac{\exp\left(\frac{\sigma_e \Omega}{RT}\right) - 1}{d^3} \tag{1.19}$$

Then with the volumetric strain taken into account Eq. 1.19 becomes:

$$\dot{\varepsilon}_D = A_D \cdot DCS \frac{\exp\left(\frac{\sigma_e \Omega}{RT}\right) - 1}{d^3} \cdot \frac{1}{e_v^{2-4}} \tag{1.20}$$

For the compaction experiments either the exact or the approximate equation will be used depending on the relationships that come out between the grain size, applied stress, volumetric strain, and temperature. For now the assumption will be made that $\frac{\Delta C}{C_0} < 1$. Therefore, Eq. 1.17 can be rewritten as a function of temperature, grain size, volumetric strain, and applied stress assuming that the pore fluid is at atmospheric pressure:

$$\dot{\varepsilon} = A_X(T) \frac{\sigma^n}{d^p} \cdot \frac{1}{e_v^q} \tag{1.21}$$

Where Ω, Z* (=DCS), and R were incorporated into A_X. This can be rewritten as:

$$\log \dot{\varepsilon} = \log A_X(T) + n \log \sigma - p \log d - q \log e_v \tag{1.22}$$

From which it is clear that in log-log plots of $\dot{\varepsilon}$ versus the stress, grain size, and volumetric strain give straight lines at a constant temperature. The slopes of these plots have been determined experimentally to be as follows for IPS:

- n = 1 for dissolution, diffusion, and precipitation controlled PS
- p = 1 for dissolution and for precipitation control, p = 3 for diffusion control
- q = 1 for dissolution control, q = 2 for diffusion and precipitation control (EXCEPT when grains are cubic it has been found that then q = 2 for dissolution and q = 4 for diffusion and precipitation control.

Thus each rate controlling mechanism, either diffusion, dissolution, or precipitation, is predicted from each unique relationship between the strain rate and the grain size used, the amount of stress applied, and the amount of volumetric strain that occurred. The compaction experiments done are carried out in such a way that all parameters are constant except one. For instance the grain size was constant for 9 experiments to find the relationship between the strain rate and applied stress. Furthermore, the grain size was varied for another 4 experiments while the applied stress was constant in each experiment to find the relationship between the stain rate and grain size. Temperature was always constant at room temperature.

2.2. Derivation of Z, the diffusivity through the NaCl-glass boundary, for the electrical conductivity experiment*

2.2.1. Theory and practice

The setup of the experiment is based on the original setup designed by de Meer et al. [de Meer et al., 2002]. It is composed of a single circular NaCl crystal positioned in a sealed miniature loading cell. In the centre of the crystal, a conical hole has been drilled in which a conical lens is pressed into. This forms the NaCl-glass contact. Above and below the crystal are two small reservoirs containing a saturated NaCl brine solution (See image 3) in where, there are also two platinum coated electrodes positioned one in each reservoir. Via these electrodes the electrical resistivity can be measured across the only pathway for the brine solution to go which is via the NaCl-glass contact. The contact has a mean radius of r and width w. A force of 2 N is then applied on the contact via spring loading (see image 3). The expected process to occur at the NaCl-glass contact is active pressure solution, which is the dissolution of the salt at the NaCl-glass contact, diffusion out of the contact, and precipitation just outside the contact making it gradually increase in width. The theory is based on the relationship between the diffusion of salt ions through the NaCl-glass contact and the electrical resistivity that are proportional to each other. The latter can be measured. Other than that there is of course also the dependence on the amount of force applied, temperature, shape and size (i.e. radius and width) of the contact, and the internal resistance in various components of the experiment. Using the Nernst-Einstein equation, the radial contact resistance can be related to Z*=DCS, the diffusivity constant, within the dissolving contact.

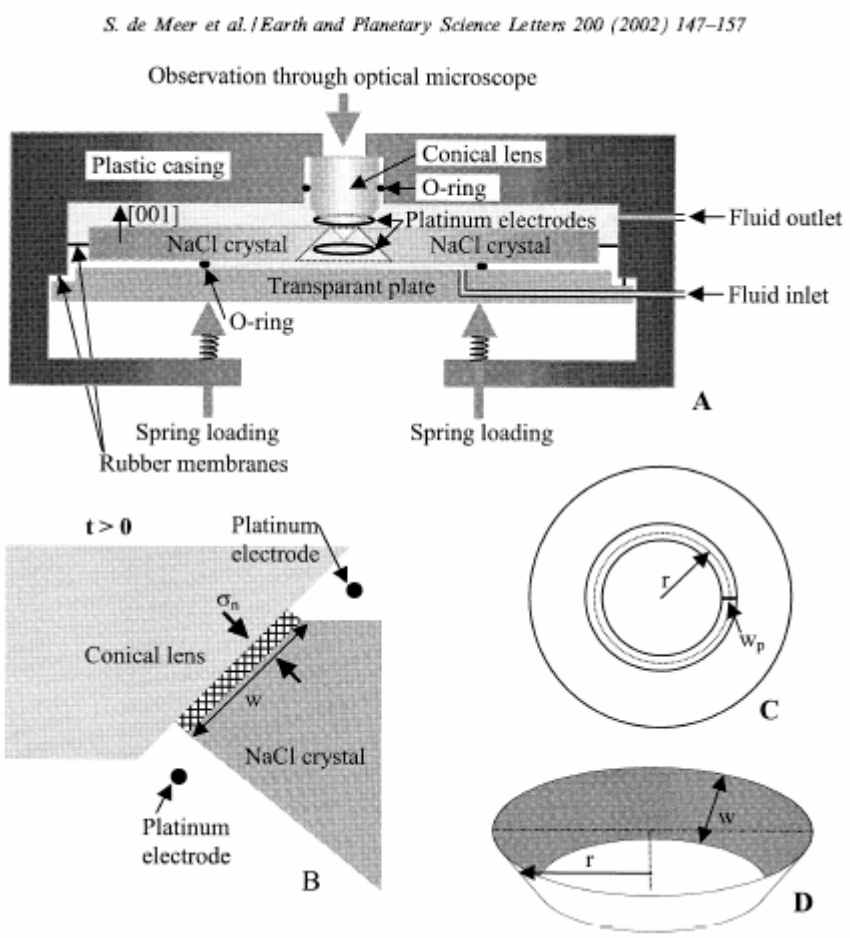

Image 3. Schematic diagram of the experimental configuration. (A) Experimental cell: axial section through the flat cylindrical body. At t =0, the NaCl disc (diameter 25 mm) just touches the conical lens forming an annular contact. (B) Close-up section of NaCl-lens contact after the start of the experiment (t > 0): an NaCl-glass contact is formed by pressure solution under normal stress σ_n with progressively increasing width w and average fluid thickness S. Note that the only path for conduction between the two platinum electrodes is through the NaCl-glass contact, i.e. through the diffusion path for pressure solution. (C) Vertical view of contact through lens at t > 0, where w_p is the horizontal projection of contact width w. (D) Three-dimensional form of the dissolving contact at any time t > 0, where r is the radius from the lens axis to the contact at w/2. Taken from de Meer et al. [de Meer et al., 2002].

2.2.2. From the Nernst-Einstein equation to a relationship involving the diffusivity constant Z*

The Nernst-Einstein equation relates the limiting molar conductivity (Λ_m° in Sm^2/mol) of an electrolyte solution to the diffusion coefficient of the dissolved charge carrying ions. It is written as follows:

$$\Lambda_m^\circ = \frac{F^2}{RT}\left(v_+ z_+^2 D_+ + v_- z_-^2 D_-\right) \qquad (1.23)$$

Where F is the Faraday's constant, R is the gas constant, T is the absolute temperature, v_+ and v_- are the numbers of cations and anions per formula unit of electrolyte, z_+ and z_- are the charge numbers of the cations and anions, and D_+ and D_- are their diffusion coefficients. In this case the NaCl brine solution is a strong electrolyte because it gives a 100% yield of ions when dissolved in water, namely Na^+ and Cl^- cations and anions. Furthermore, the solution is assumed to be almost completely dissociated, meaning that few NaCl compounds are left behind. In the first approximation, the ions move independently during

conduction, and the conductivity is expected to be proportional to concentration. An approximately concentration independent quantity, the molar conductivity Λ, can be defined in SI units by dividing the conductivity by the concentration in mol/m^3:

$$\Lambda_m^\circ \approx \Lambda_m = \frac{\kappa}{C_m} \tag{1.24}$$

Where κ is the conductivity of the solution (Sm^{-1}) and C_m is the concentration of the NaCl in solution (mol/m^3). Also, because the salt solution is nearly completely dissociated, the sodium and chlorine ions start to form hydration spheres, meaning water molecules will start to surround the cations and anions. In addition, because we are dealing with a NaCl-glass contact the diffusion coefficients D_+ and D_- become effective diffusion coefficients, or 'normal' diffusion coefficient plus 'pore characteristics.' That is, in real pore systems there exist windings, contractions, crossings and so on. It will be necessary to correct the 'ideal' diffusion coefficients by a factor to get the so called 'effective diffusion coefficients', which represent the system with real pore geometry. It has been shown that a correction factor which is the porosity of the material divided by a so called tortuosity factor is sufficient for most cases. Due to the properties of Na+ and Cl- ions, the following equations hold:

$$\begin{aligned} v_+ &= v_- = 1 \\ z_+ &= z_- = 1 \\ D_+ &= D_- \end{aligned} \tag{1.25}$$

Moreover, the brine solution is saturated as mentioned before. This means that the concentration of NaCl in the solution is equal to the solubility of NaCl (m^3/m^3) divided by the molar volume of NaCl (m^3/mol):

$$C_m = \frac{C}{V_m} \tag{1.26}$$

Therefore the conductivity of 'a near' saturated brine phase in a NaCl-glass contact undergoing pressure solution can be written as:

$$\kappa = \frac{2F^2 D C_m}{RT} \tag{1.27}$$

In the experimental setup, the quantity that is measured is Ω or the resistance of the narrow annular contact (see Image 3). Ω is related to κ via the width of the NaCl-glass contact divided by the circumference of the cone (2πr) multiplied by the average thickness of the fluid in the contact, S and the conductivity κ in the contact:

$$\Omega = \frac{w}{2\pi r S \kappa} \tag{1.28}$$

Where *w* and *r* are the width and average radius of the circular contact respectively. At this point again an important assumption is made this time regarding the pore geometry in the NaCl-glass contact. As said before, for a correct representation of the system with real pore geometry a correction factor must be applied which equals the porosity divided by the tortuosity factor. In this case it is assumed that there is negligible tortuosity in the internal conduction path. Finally, combining Eq. 1.28 with Eq. 1.27 with Eq. 1.26 and that Z* = DCS the following expression is obtained that represents the diffusivity through an NaCl-glass contact:

$$\kappa = \frac{w}{2\pi r S \Omega} = \frac{2F^2 D\left(C/V_m\right)}{RT}$$

$$wRTV_m = 4\pi r S \Omega F^2 DC$$

$$DCS = \frac{V_m RTw}{4\pi r F^2 \Omega}$$

$$Z^* = DCS = \frac{V_m RT}{4\pi F^2} \cdot \frac{w}{r} \cdot \frac{1}{\Omega} \qquad (1.29)$$

Where $V_m RT/4\pi F^2$ is a constant at constant temperature and R = 8.314472 m^2 kg s^{-2} K^{-1} mol^{-1} and F = 96 485.3415 Coulombs. Also important to note is that the resistance of the open solution between the electrodes and the contact is by far insignificant compared to the resistance measured across the NaCl-glass contact and can thus be neglected. Ω can be easily measured and thus Z* can be calculated.

This is the same quantity that has been derived in section IIa on the derivation of the strain rate equation for intergranular pressure solution (IPS) for the compaction experiments. These will then be compared at the end.

3. Materials and methods

3.1. Compaction experiments

The experimental setup was originally designed by C. Spiers from Utrecht University, The Netherlands [Spiers and Brzesowsky, 1993]. It is a very simple setup for studying pressure solution of compacting halite at room temperature and at pressures ranging from 0.82 MPa upto 5.81MPa as in this experiment.

3.1.1. Procedure

Various compression experiments were carried out using grain size and stress as variables, whereas temperature was always constant at room temperature. Many combinations were tried keeping either the grain size constant or stress in order to verify the relationships that would exist if the compaction process were occurring via pressure solution. The experiments can be divided into several categories as seen in table 1; dry compaction, constant grain size (at 35 microns) wet compaction, and constant stress (at 5.81 MPa) wet compaction experiments. Note that for these experiments most were carried out with a very small grain size as opposed to the experiments carried out by Spiers et al. (1993), where grain sizes were used ranging from 98 μm to 410 μm.

Table 1 List of experiments performed showing the temperature, grain size, applied stress, initial salt column length and the total strain

Experiments	T (°C)	d_r (μm)	d_c (μm)	d_s (μm)	Mass of weights* (g)	σ_e (MPa)	L_0 (mm)	Total strain (%)
DC 1	22	150	134	167	466	5.81	9.8	-
WC 1	22	35	30	37	466	5.81	9.85	19.73
WC 2	22	35	30	37	366	4.55	9.6	16.55
WC 3	22	35	30	37	266	3.32	11	14.27
WC 4a	22	35	30	37	166	2.05	10.25	14.81
WC 4b	22	35	30	37	166	2.05	10.25	13.77
WC 5a	22	35	30	37	116	1.45	9	10.05
WC 5b	22	35	30	37	116	1.45	10.5	11.70
WC 6a	22	35	30	37	66	0.82	9.8	11.04
WC 6b	22	35	30	37	66	0.82	10.6	12.36
WC 7	22	85	74	92	466	5.81	10.6	12.92
WC 8	22	150	134	167	466	5.81	10	8.66
WC 9	22	160	140	175	466	5.81	9.8	3.18

DC 1 denotes dry compaction, *WC #* denotes wet compaction at constant grain size, and **WC #** denotes wet compaction at constant stress. T denotes environment temperature, d_r reported grain size, d_c corrected grain size cubic, d_s corrected grain size spherical, σ_e applied stress, L_0 initial length of salt column. *Force exerted by dial gauge added an extra 647.5N (=66g).

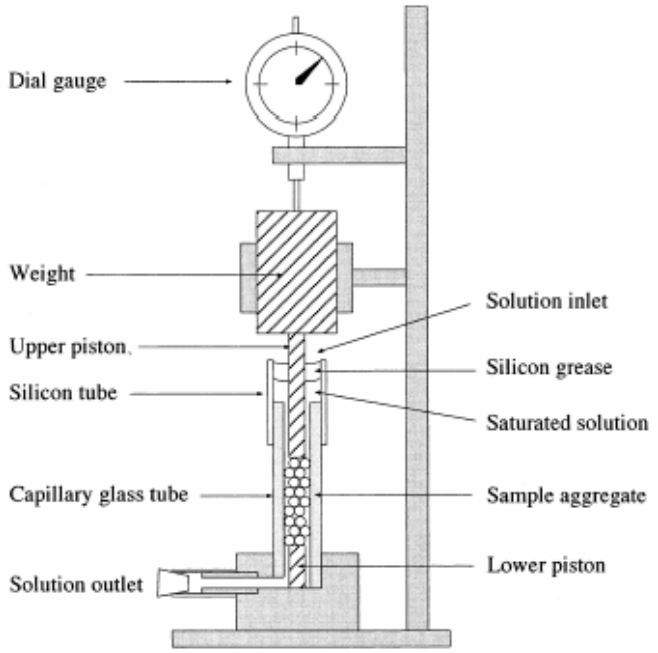

Image 4. Schematic drawing of the experimental set-up used for wet compaction of NaCl aggregates. Taken from den Brok et al. [den Brok et al., 1999]

The apparatus was set up according to Image 4. The capillary tube was placed in the brass base and a shorter steel piston was inserted in it. Then the capillary tube was filled with about 1 cm of salt powder starting with salt 35 micron in diameter. Then the longer steel piston was inserted into the capillary tube onto the salt powder. Lastly, the plastic collar was placed on the capillary tube. The initial compaction of salt was started using an initial 500 grams of weights and the compaction process was left going for 2 minutes. This was repeated for other grain size/stress experiments because this will give the same initial starting porosity. After 2 minutes the weight was reduced to the desired amount position the dial gauge above it and zeroed at the 5mm mark. Then carefully the height (L_0) of the salt column was measured using the calliper. The experiment was left going for another 5 minutes. After that time the dropper was filled with some of the brine solution and the solution was added in the plastic collar and drawn into the sample by carefully sucking on the "evacuation tube." At the same instant the stop-watch was started. The same was done for the other experiments, which were monitored for displacement versus time for about 1500-2000 seconds depending on the speed of the pressure solution process. Every 20 seconds the position of the meter on the dial gauge was recorded.

From this data the cumulative displacement (X) was calculated (in mm) and plotted against time (t). It is important to realise that the total applied stress is the weight of the brass weight plus the amount exerted by the dial gouge (= 66g at the 5 mm mark). From this data the length of the salt column was calculated ($L = L_0 - X$) at any instant in time, the volumetric strain ($e_v = X/L$) and the strain rate ($\dot{\varepsilon} = (dX/dt)/L$).

Using the data, plots of log(ε rate) vs log(e_v) and plots of log(ε rate) vs log(d) and log(ε rate) vs log(σ) at constant strain were constructed. The slope in these plots confirm what the rate limiting process is in pressure solution, be it dissolution, diffusion, or precipitation.

3.1.2. Grainsize verification procedure:

Because salt quickly reacts with the moisture in the air, small grains may clump together forming bigger grains. This has an adverse effect on the experimental results. In order to make sure the grain size is correct a simple procedure can be used. A tiny amount of salt grains were placed on the slide which was carefully positioned under the microscope. All grains were counted and then, without loosing any grains, they were weighted on a sensitive balance. Knowing the mass of all the grains and the number of grains, the mass of a single grain was calculated. Knowing the density of NaCl, the volume of the grain was calculated. From that the grain size can be deduced, whether it is cubic or spherical.

3.2. Electrical conductivity experiment on the [100] plane of an NaCl crystal

This experiment is nearly identical to the one made by S. de Meer, C. Spiers, C. J. Peach, and T. Watanabe in 2002. The only differences are that the hole in the NaCl crystal is comparatively smaller by about 300μm in diameter and a different force was used, this time about 2N. See table 2.1 below.

Table 2 Details of the experiment

Experiment	Applied force	Radius, r_0 of hole in crystal	"Current sense resistor", R_I	Duration of exp.	Ambient temperature
Exp. 1	2 N	~470μm	100 kΩ	11 days	(26-27)°C

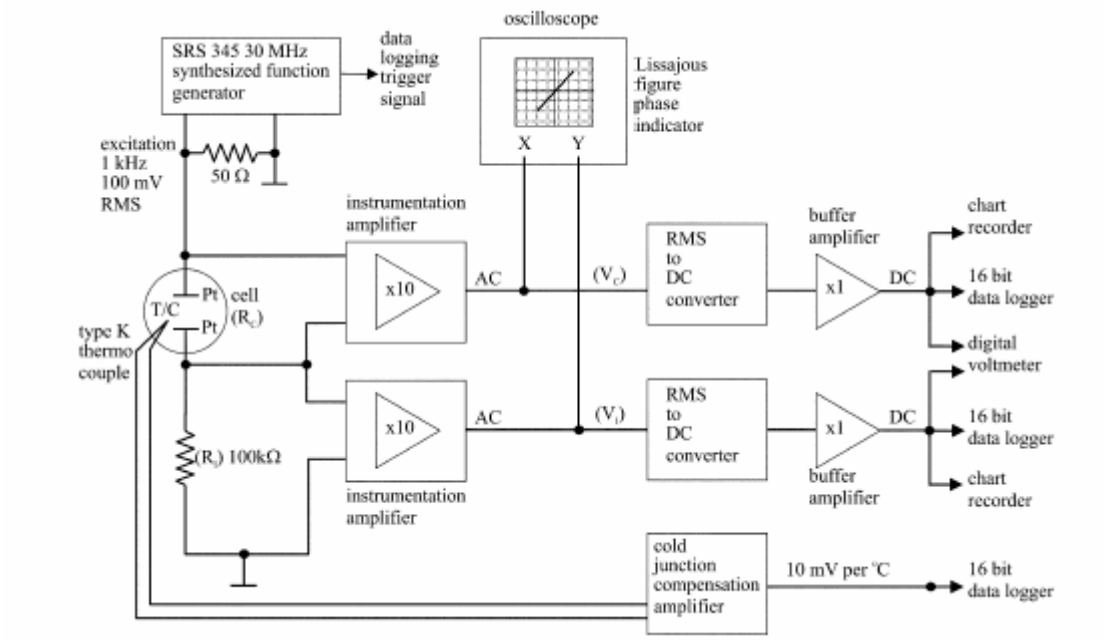

Image 5. Schematic diagram of experimental setup used to measure the resistivity of the conduction path between the two platinum electrodes. Taken from de Meer et al. [de Meer et al., 2002].

See Image 3 for the experimental setup. The experimental cell consists of two fluid reservoirs containing an NaCl brine solution and the cell is separated by a salt crystal. In the middle of the crystal a cone shaped indent exists where the glass cone will cut into. This is the NaCl contact boundary where pressure solution will occur. Above and below the crystal are two platinum electrodes positioned that will measure the electrical resistivity in the brine solution. The only path the ions in the brine solution can flow is via the NaCl-glass contact. A force of 2N is applied to the contact by means of three adjustable springs, calibrated by replacing the glass lens with a push-rod linked to an electronic balance. The temperature is measured using a type K thermocouple placed close to the NaCl-glass contact. The NaCl crystal used came from a cylindrical mother crystal. Using machinery a conical hole was cored in the small cyclindical crystal parallel to the [100] crystal plane and was about 1-2 mm diameter at the contact. It was then annealed at 700°C for 20 hours to remove dislocation damage producing a smooth unscratched surface all around. The platinum electrodes were coated with platinum black to minimise polarisation effects. Image 5 shows how the electronics was setup.

The apparatus was first assembled with the crystal sufficiently retracted to avoid contact with the lens. The lens was then pre-loaded at 2 N before initiating wet testing. After dry-loading, the load was removed to allow the contact to fully reopen. The brine solution was then added into the cell via the lower reservoir with the fluid outlets closed. The load of 2 N was added again via spring loading causing the brine in the cell to become pressurised. By bleeding out the excess brine solution via the outlets, the conical lens and the rim of the central hole were brought into contact. At this point a programmable digital signal generator was started sending a 1 kHz sine wave burst to the platinum electrodes every 1000 s. The sine wave had a 3 second duration and 283 mV RMS amplitude. The alternating current (AC) flowed via a 'current sense resistor' R_1, of 100kOhms. Across this resistor the voltage dropped. V_1 and cell, Vc were amplified and measured. This was done via RMS to direct current (DC) converters giving simultaneous logged values of voltage and current. From V_1 and Vc the resistance of the cell was calculated using Ohm's law: ($Rc = Vc * R_1/V_1$). All voltages, including that from a type K thermocouple representing the cell temperature, were logged every 500 s to 16 bit precision on a computer via an analogue to digital converter. The widening of the loaded contact was followed by taking digital

photographs of the contact via an optical microscope combined with a digital camera. The photographs are essential for measuring the width, w and the radius, r of the contact as a function of time, with a correction for refractive index effects. Note that an initial photograph was taken of a grid only with known width for reference of scale. In this case 1 square has the width of 0.4 mm. Because the circular field of view in the microscope is unaltered, the scale on each photograph of the NaCl contact can be deduced.

The entire experiment took 11 days at a relative constant temperature between 26°C -27°C. The force used was 2 N causing a normal stress acting on the contact ranging from 1 to 8 MPa. Whenever possible, two pictures were taken in one day. The rate of pressure solution could not be accurately calculated because the displacement of the crystal relative to the lens could not be measured accurately enough. The surface structure of the crystal after the experiment was not investigated either. The integrity of the crystal surface area could not be guaranteed when extracting the crystal from the cell.

As it turned out, the computer had failed to log the voltages send to it. This would have meant a failed experiment were it not for the graphical logger attached to the set up. It produced a graph of V_l and cell, Vc respectively. It recorded 0.1 mm every minute. So that would be 1 cm every 6000 seconds. After careful inspection of the graph, it occurred to me that 12 measurements were taken in 1 cm for a total of 156.2 cm. This means that the rate of measurements taken would be one every 500 seconds (=6000/12). The experiment took 11 days (=264 hours in 156.2cm), so 1 hour is 0.5909 cm. From this a time scale was created on the graph and measured V_l and cell, Vc every 6 hours (=3.54 cm). Having done that a plot of Rc versus time was created including the moments when the pictures were taken using the digital camera in the microscope.

The plots which were created were contact resistance (Rc) versus time and versus normalised contact width (w/r) plots and effective grain boundary diffusivity (Z*) versus grain contact width (w) and Z* versus normal stress across contact plots. The normal stress was calculated from the geometry of the NaCl-glass contact. The normal force is equal to $\sigma_n = mg\cos\vartheta$, where mg = 2 N and $\vartheta = 45^\circ$ (the angle of the cone against the NaCl crystal). Across the entire conical area, the area is equal to $A = \pi \cdot (R + r)w$, where R is the upper radius and r equal to the lower radius of the sawed off cone and w the contact width. The average normal stress would be 2N / A.

4. Results

4.1. Compaction experiments with granular NaCl

The first experiment that was carried out was with dry compaction of granular salt with a grain size of about 150 ± 16 μm. As expected there was only some initial compaction that took place with the standard 500 grams. But after that when the amount of mass (i.e. stress) was adjusted (to 466 grams), no further compaction was seen on the dial gauge.

On the other hand, the wet compaction experiments showed considerable strains or creep as time progressed. See Figure 1 and Figure 2 for instance. Both figures show how there is firstly relatively rapid creep followed by a steady decrease in the creep rate. Notice that in Figure 2 the lowest curve does not necessarily compare with the lowest applied stress, although it is intuitive that the smaller the applied stress, the smaller the volumetric stain should be.

The data that has been obtained from the wet compaction experiments will demonstrate the relationship of the strain rate, $\dot{\varepsilon}$ upon applied stress, σ_e, grain size, d, and the volumetric strain, e_v.

The next figures, Figure 3 and Figure 4 show the relationship between strain rate and the volumetric strain for different grain sizes and different stresses consecutively. Note that the slope is close

to a value of 2 except for the data of grain size of 160 ± 15 micron. From observation of Figure 3, it looks like it probably will go to 2 at lower strain rates. For Figure 4 the relationship is very consistent for each experiment and the slope overall is clearly 2. Only the 5.81 MPa experiment shows a slight deviation. Also note that it is not necessarily true that the lower the applied stress, the lower the volumetric strain as shown. Overall, the strain rate can be said to be roughly in proportion to $1/e_v^c$, where c is 2. At higher values of e_v, the sensitivity of $\dot{\varepsilon}$ increases.

Figures 5 and 6 show the strain rate plotted against the grain size. Especially in Figure 5, the relationship is very clear with a slope of 3. But also Figure 6 quite convincingly shows that there is a clear correlation between $\dot{\varepsilon}$ and d. The figures could not be merged because the data had to be plotted at a constant e_v. The volumetric strain of the data with an average grain size of 35 micron could not be compared with e_v from the data from the experiment using an average grain size of 160 ± 15 micron.

The last figure, Figure 7, shows the relationship of strain rate versus applied stress. It illustrates that at constant grain size and strain, the relationship is linear with a slope just a bit higher than 1. For lower stresses retakes were done in order to test the imprecision of an experiment and to confirm the slope is actually close to 1 and not less. For all three cases the deviation shows to be about 1 order of magnitude.

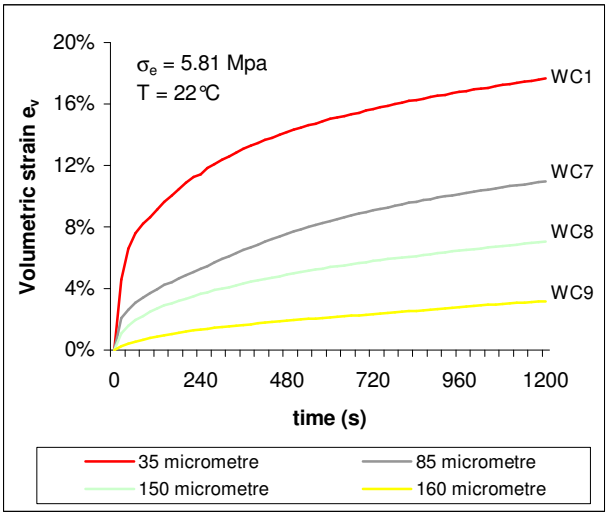

Figure 1 Volumetric strain versus time plot for different grain sizes

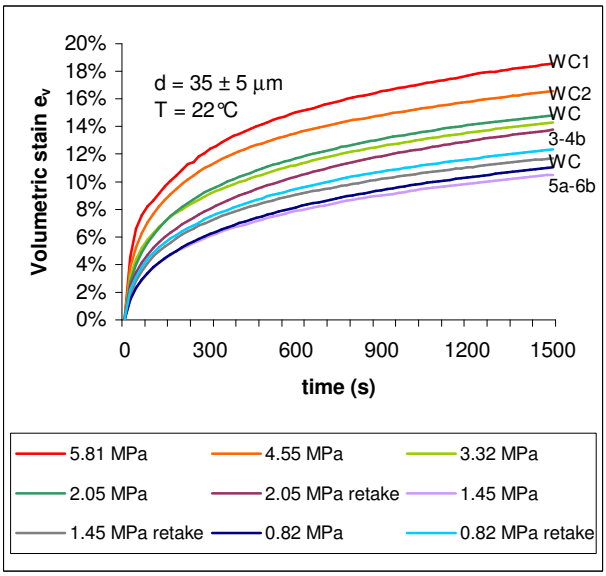

Figure 2 Volumetric stain versus time plot for different stresses at constant grain size.

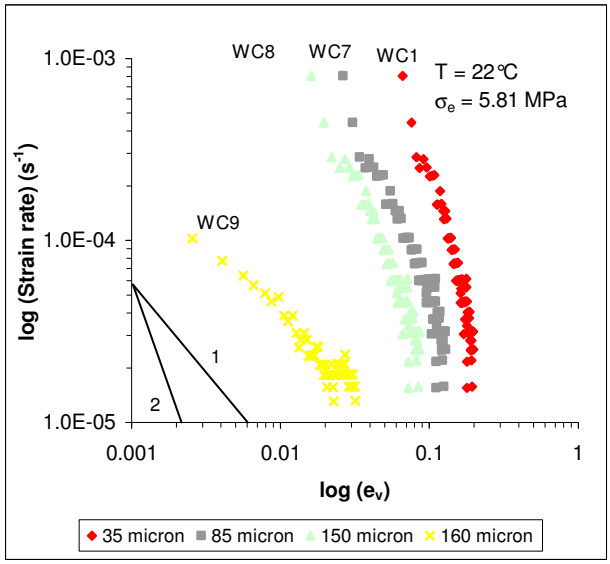

Figure 3 Log-log plot illustrating the dependence of compaction strain rate on volumetric strain (ev) at constant stress and temperature

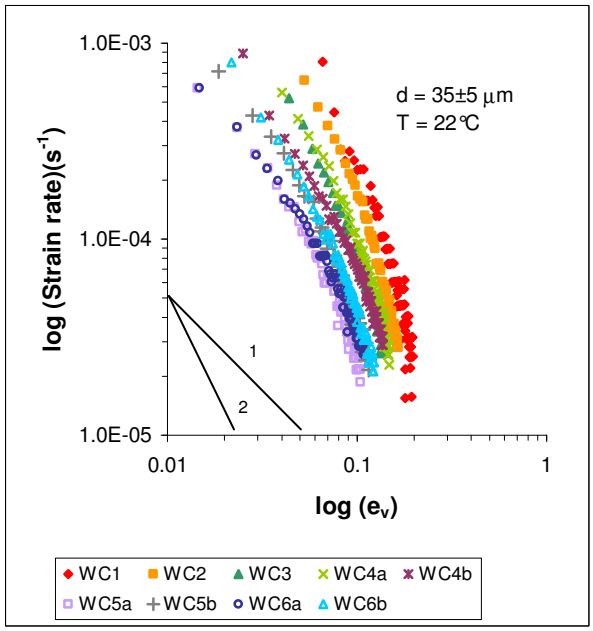

Figure 4 Log-log plot illustrating the dependence of compaction strain rate on volumetric strain (ev). Grain size is constant at 35 µm, temperature at 22°C.

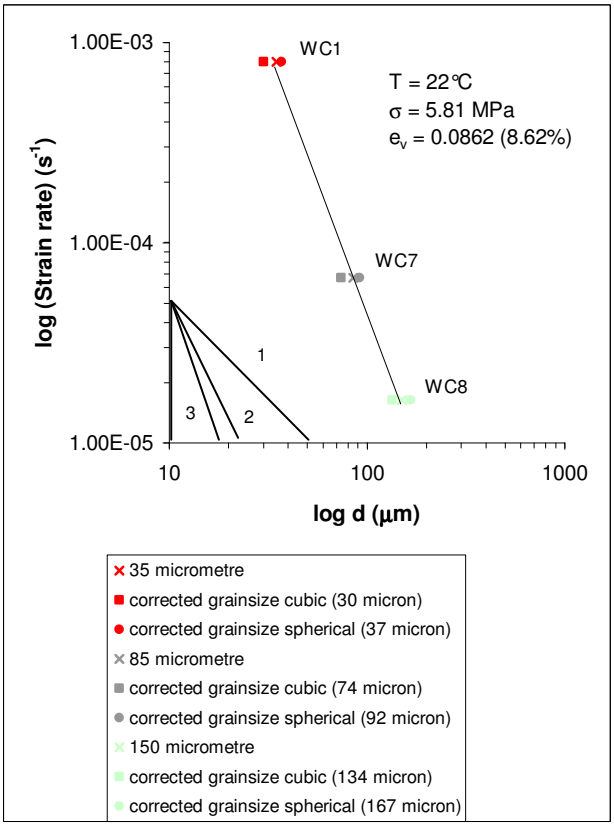

Figure 5 Log-log plot displaying the dependence of compaction strain rate on grain size (d) at constant stress and strain.

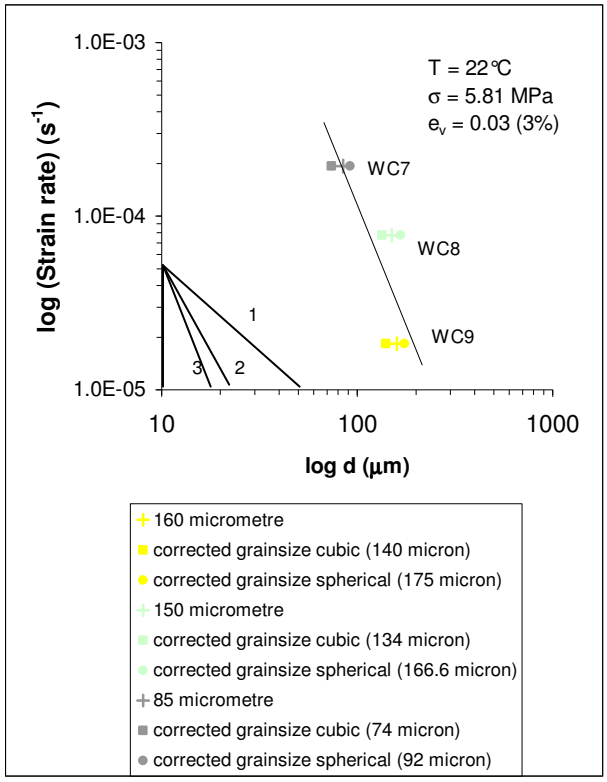

Figure 6 Log-log plot displaying the dependence of the compaction strain rate on the grain size (d) at constant stress and strain

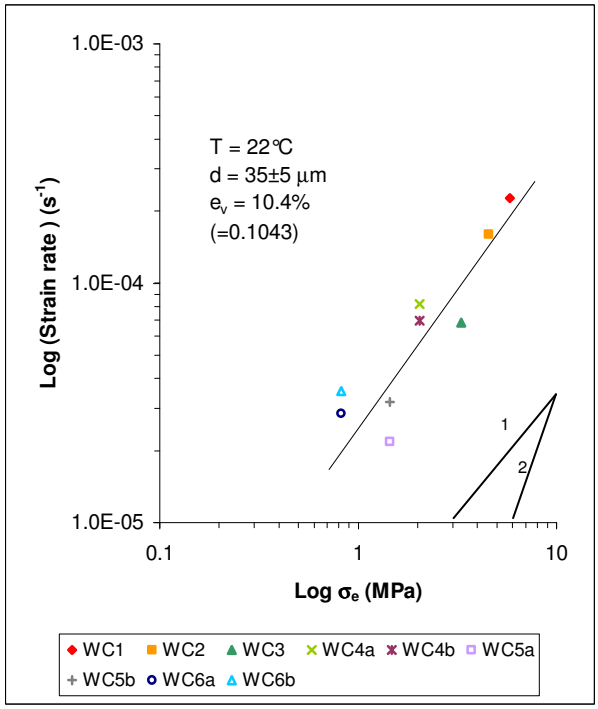

Figure 7 Log-log plot portraying the dependence of the strain rate on the applied stress (σ_e). Grain size, temperature, and strain are constant.

4.2. Electrical conductivity experiment on [100] plane of an NaCl crystal

4.2.1. Optical results

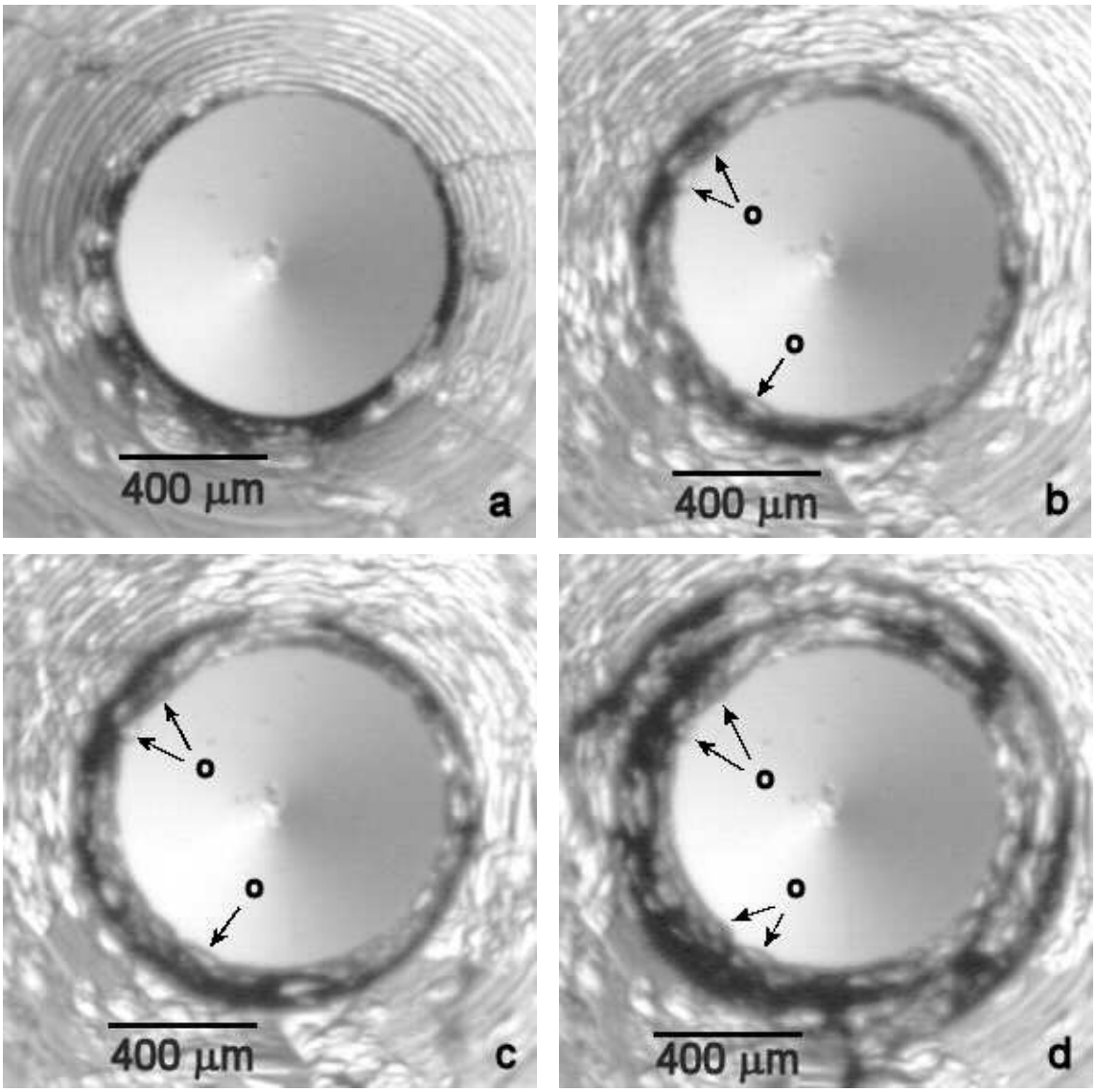

Figure 8

Micrographs taken of the NaCl-glass contact through a camera mounted on an optical microscope at different moments in time. Temperature slightly fluctuated between 26-27°C and applied force was constant at 2 N. (a) Start of experiment after the brine was added and the logging began; (b) contact after about 4 days; (c) after about 7 days; and (d) after about 11 days at the end of the experiment. 'o' indicates overgrowths.

Observations from micrographs

At the instant the experiment was started a black ring already formed around the central cone, noticeably very irregular in width (see Figure 8a). The ring continued to grow, but became remarkably uniform in width (see Figure 8 b,c) until something happened that caused the ring to expand very rapidly as seen in micrograph (d) where curiously a second ring has formed, three quarters around the cone. Normal stresses at the contact range from ~7.5 MPa at the beginning to ~1.5 MPa at the end of the experiment. In Figure 8 b, c, and d overgrowths can also be observed on the free surfaces close to the crystal-lens contact and on the (001) top surface of the crystal (indicated by 'o'). The concentric optical modulations seen within and outside the dark ring contact are roughness developed on the machined conical surface of the NaCl crystal below the focal plane and not within the contact itself. This is verified by the fact that the rings become increasingly out of focus away from the contact and existed before the experiment got started. Due to the way the experiment was set up, the NaCl-glass contact could not be investigated in detail.

In the micrographs below you can see how a front is forming and moving towards the centre where the ring is located. From the way it looks, it is probably newly precipitated salt forming a new surface on the NaCl crystal.

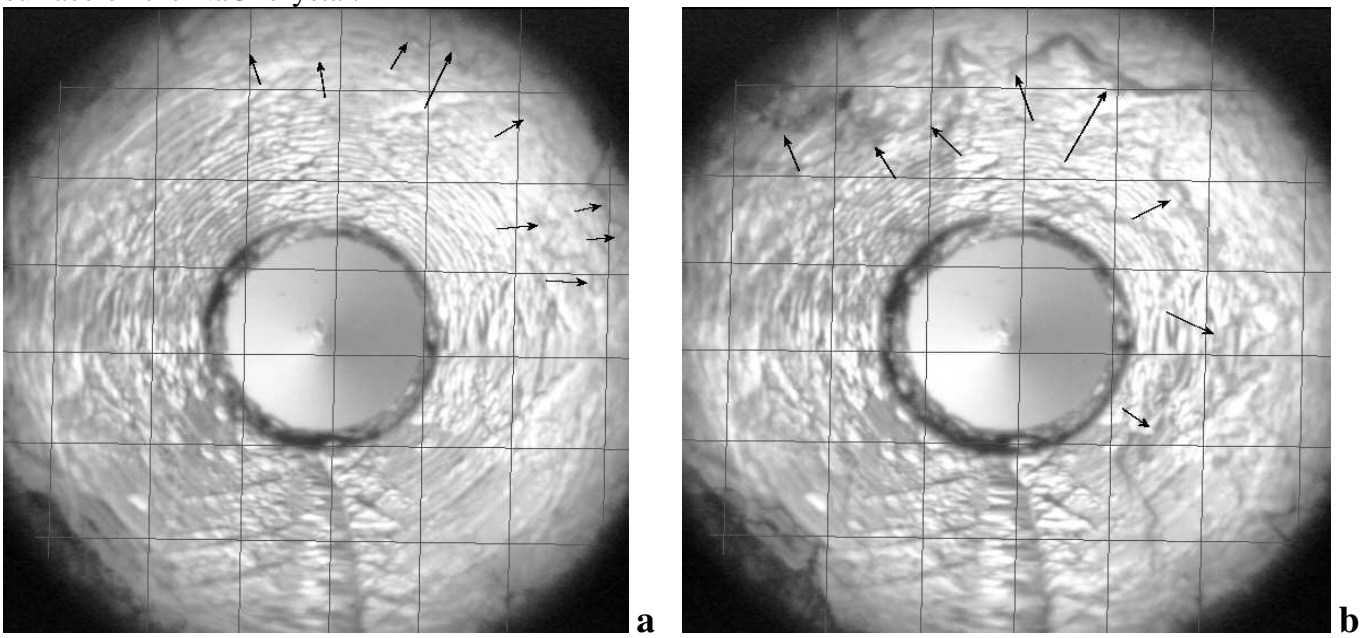

Figure 9

Two micrographs where dark lines are advancing across the (001) plane of the NaCl crystal. (a) was taken after about 4 days and (b) after about 6 days. The width of one square is about 0.4 mm (or 400 micron) in the NaCl-glass contact region.

Then lastly, in the earlier micrographs an important detail is seen which must not be overlooked. Figure 10 is a micrograph taken at day 2 in which clearly three pathways can be seen going from the dark ring in the centre towards the edge of the micrograph. To be interpreted in section V, b.

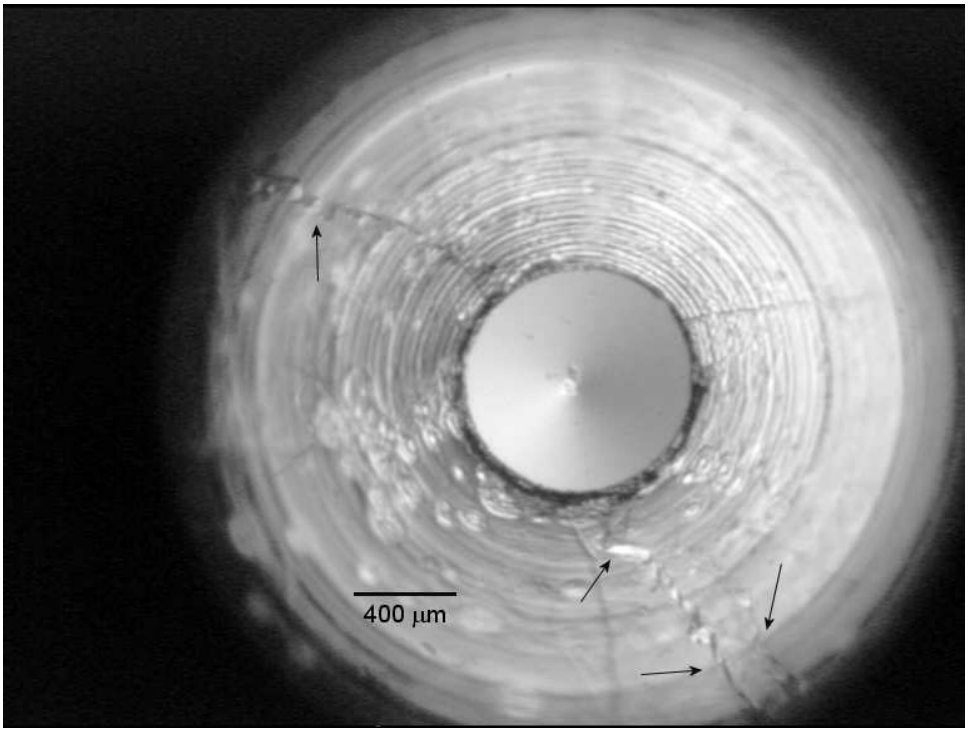

Figure 10

A micrograph taken at day 2. Arrows indicate the three pathways. The elliptical shapes on the crystal surface are most likely air/silicon oil pockets.

4.2.2. Graphical results

Figure 11 Plot of contact resistance versus time at constant temperature and force. is a plot of the contact resistance versus time curve at constant temperature and applied force. The contact resistance starts at zero and remained at there until day three when the contact resistance started to increase. Half way during day four, however, the contact was opened again causing the contact resistance to drop. From day five, however, a very large resistance peak had finally formed with the maximum of ~628 kOhm at day seven. Afterwards the contact resistance dropped again to a plateau at ~80-70 kOhm.

In Figure 12 Log-linear plot of contact resistance versus normalised contact width., it is evident that there is no clear relationship. And in fact the linear relationship predicted by Eq. 1.28 is not obtained. The resistance shows to be unrelated to w/r. However, it is important to note that this data mostly comes from the point where the contact was not formed yet. Only the last 3 data points come from after the peak seen in Figure 11 Plot of contact resistance versus time at constant temperature and force..

Using Eq. 1.29, the contact radius and width data from the optical micrographs as a function of time, the resistance data has been recalculated to find the various corresponding Z* – values. These processed results, applicable to pressure solution in NaCl, were used to plot graphs of Z* versus the contact width (Figure 13 Log-linear plot of the logarithmic diffusivity, Z* versus the grain contact width, w. and Z* versus the normal stress, σ_n (Figure 14 Log-log plot of the diffusivity versus the normal stress acting on the NaCl contact.). All data points in both figures correspond with the moments pictures were taken (see Figure 11). Figure 13 shows that with increasing contact width w, Z* also increases. Because the contact width is correlated with the area of the contact and applied force is constant at 2N, Z* must also be related to the normal stress at the contact. This is demonstrated in Figure 14 Log-log plot of the diffusivity versus the normal stress acting on the NaCl contact. This figure illustrates how normal stresses in the range 1 to 8 MPa, Z* are inversely proportional to σ_n. Figure 15 is similar to Figure 14 except that additional data is plotted in it from previous experiments, mainly from de Meer, et al. The data in this plot clearly show a positive correlation between Z* and w. Despite the scatter, the trend in the data with an applied load of 2N does not deviate greatly from the other data. Some points in the region with data from de Meer, et al. nicely plot at the location of 3N. Five data points corresponding with the last five optical micrographs from the present experiment plot rather higher, that is with a lower Z* value between (1E-17 to 2E-16) m^3/s than other data. In Figure 16 Log-log plot of the diffusivity, Z* versus the normal stress across the NaCl-glass contact., again it is shown that, despite the scatter of the data with an applied load of 2N, the data follows a similar trend with other data of 3N from de Meer et al. However, the points that lie in the region with a diffusivity of (1E-17 to 2E-16) m^3/s correlate with a higher normal stress than expected from the other data. They are the same five points described before.

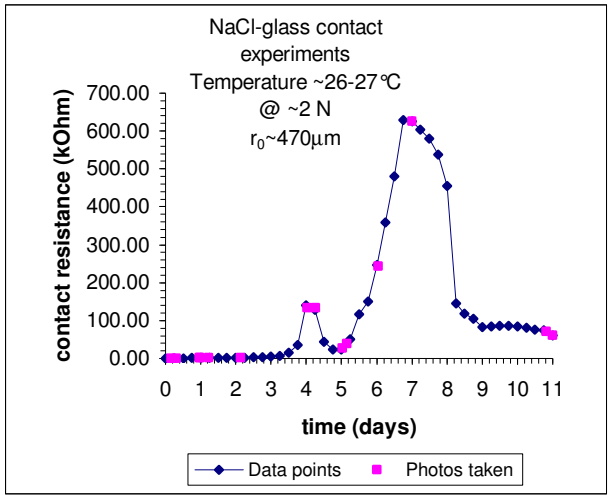

Figure 11 Plot of contact resistance versus time at constant temperature and force. The purple squares indicate the moments photos were taken used to measure contact width, w and radius, r.

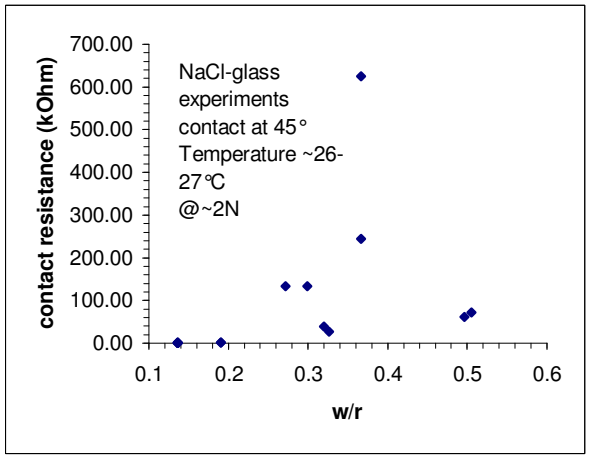

Figure 12 Log-linear plot of contact resistance versus normalised contact width.

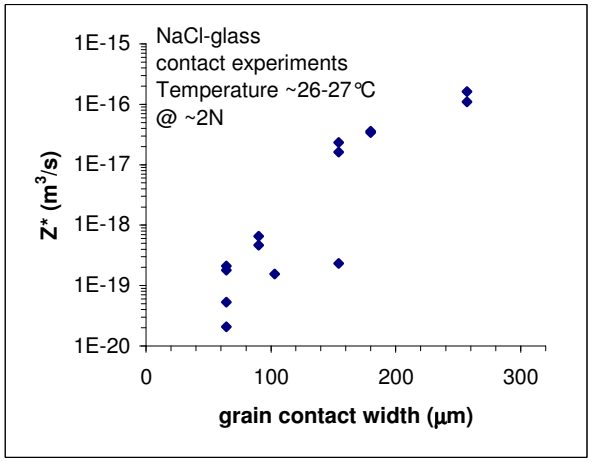

Figure 13 Log-linear plot of the logarithmic diffusivity, Z* versus the grain contact width, w.

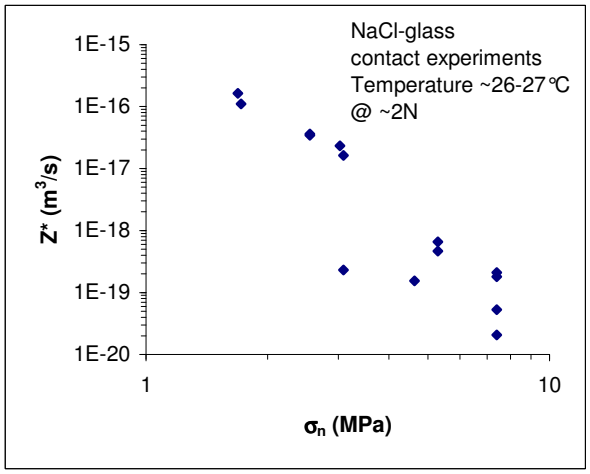

Figure 14 Log-log plot of the diffusivity versus the normal stress acting on the NaCl contact.

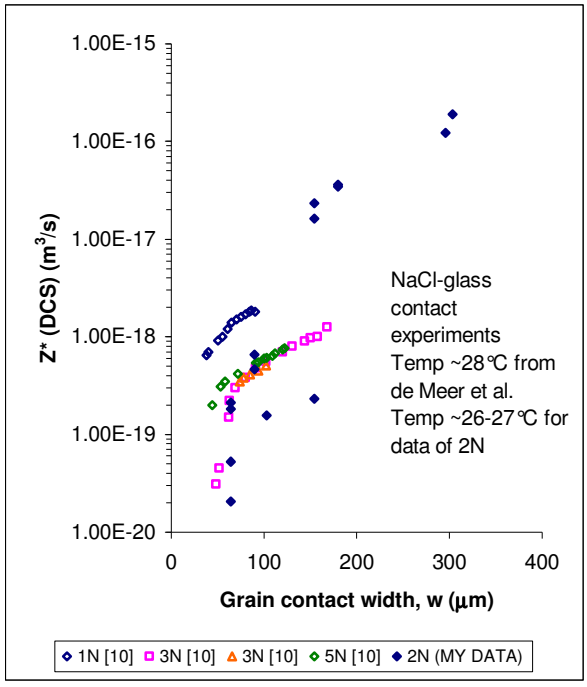

Figure 15 Log-linear plot of the diffusivity, Z* versus the grain contact width, w.

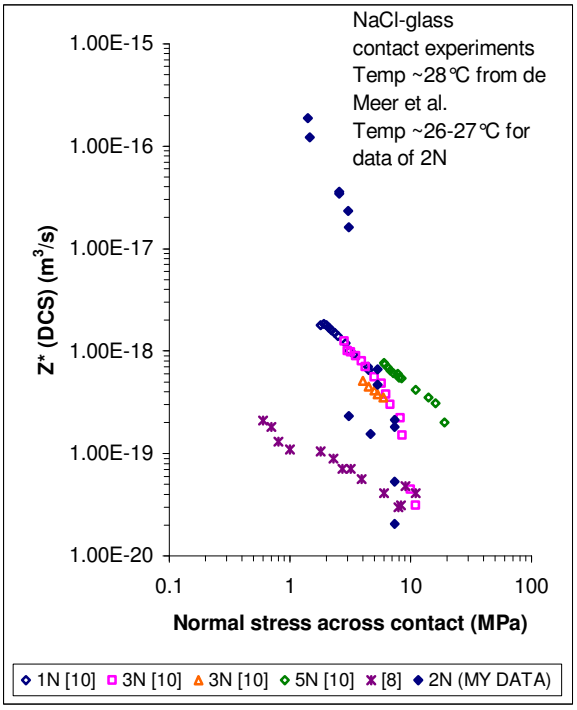

Figure 16 Log-log plot of the diffusivity, Z* versus the normal stress across the NaCl-glass contact.

5. Discussion

5.1. Compaction experiments

The compaction experiments were divided into a dry run and various wet runs. There was only need for one dry run to verify no compaction or strain took place after an initial porosity reduction caused by the weights. Compaction did take place when a drop of brine solution was added. The fact that no compaction took place for dry salt does not automatically mean that for wet salt the compaction process is pressure solution. It does mean that there are probably no effects of crystal plasticity. But instead of pressure solution there could be also another exotic compaction process taking place that satisfies the strain rate versus volumetric strain, versus grain size, and versus applied stress relationships, for example a process involving brittle behaviour. However, in previous experiments samples were prepared for microscope study and results showed that many indentations and overgrowth microstructures were formed typical for pressure solution [Spiers and Brzesowsky, 1993] except at higher applied stresses above 4 MPa. Additionally results show that the slopes in each graph where the strain rate versus the volumetric strain, versus the grain size, and versus the applied stress were plotted compare very well with the theory: $\dot{\varepsilon} \approx e_v^{-q} \cdot \sigma_e^n \cdot d^{-p}$ where $q \approx 2$, n is slightly higher than 1, and $p = 3$. Also work by De Meer and Spiers [de Meer and Spiers, 1997] showed that friction is negligible with the sample lengths used. This gives enough proof that the dominant compaction process for these experiments is pressure solution. In addition, the grain size has been double checked by taking a few hundred grains, averaging them over the mass for one grain and calculating the grain size from the volume of that grain knowing the density of salt. The grains looked more cubic under the microscope but to be on the safe side, the extremes were taken, a perfect cube as opposed to a perfect sphere. The error is very small and not very significant. E.g.

from a batch of 200 grains, and counting only 90 per cent of them, the resulting variation in grain size is only a couple of micrometres. The reported grain size shows to be fairly correct in contrast with the calculated cubical and spherical grain sizes (see Figure 5 and Figure 6)

Having established that pressure solution is the main process, from theory (see introduction) the diffusivity, Z* can be calculated which is equal to S (or grain boundary film thickness, m) multiplied by D (diffusion coefficient in the grain boundary, m^2/s) and C (the solubility of the diffusing Na^+ and Cl^- ions in the grain boundary, m^3/m^3). The average normal stress $<\sigma_n>$, can also be calculated using $<\sigma_n>= \bar{A}\sigma_e\left(1-e_v\right)^{2/3}/e_v + p$ where $\bar{A} = 6/\pi$ and p, the pore pressure is assumed to be equal to the atmospheric pressure and can be neglected [Spiers and Brzesowsky, 1993]. Thus the following graph (see Figure 17 A Log-log plot of the diffusivity Z* versus the average normal stress across the grain boundary for the compaction experiments) is produced when applying the formulas for Z* and $<\sigma_n>$ showing the relationship that exists between the two.

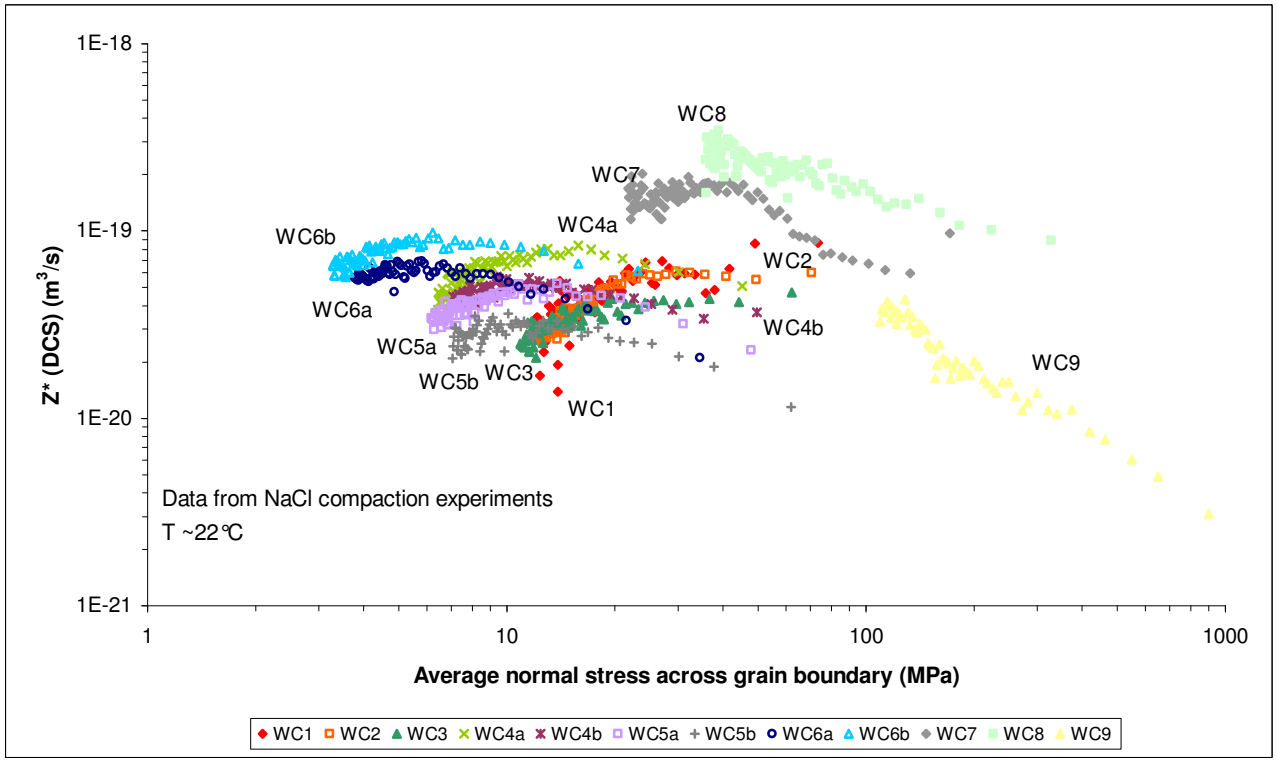

Figure 17 A Log-log plot of the diffusivity Z* versus the average normal stress across the grain boundary for the compaction experiments

Figure 17, A Log-log plot of the diffusivity Z* versus the average normal stress across the grain boundary for the compaction experiments shows that the diffusivity, Z* lies within 2 orders of magnitude from 4E-19 m^3/s down to 3E-21 m^3/s. Note that the greater the grain size, the higher the normal stresses on the grains become, see WC7, 8, 9. But it is questionable whether for experiment WC9 normal stresses close to 1 GPa are realistic. Figure 17 also illustrates that initially there is a positive relationship followed by a negative relationship at larger grain size and greater applied stress. This means that the diffusivity, Z* across the grain boundary first increases with increasing $<\sigma_n>$ then at a certain moment the opposite happens. One possible explanation is that either S increased with time, D, or C. Most certainly C, the solubility of the diffusing species, i.e. NaCl did not change. The fluid film thickness, S could, however,

have changed with time. Several authors argue that the mean intergranular fluid thickness, S may be stress dependent [Hickman and Evans, 1995 , Rutter, 1983 , Renard et al., 1997]. They also argue that D and C may be related to S. Thus film thickness initially has grown in relationship with increasing normal stress. Note that this process can only take place if the grain boundary fluid is thin enough for surface forces to play a role. Normally this is only possible if the grains are small enough. The process may be the precipitation of NaCl in the grain boundary contacts from the edges of the grains via pressure solution. This causes the fluid film thickness to first increase. Also as the edges of the grains dissolved away, the grain boundary contacts between the grains would become smaller, i.e. less area, which means a greater normal stress on the contact. Then at a certain moment the process reversed and dissolution started to occur in the NaCl-NaCl grain contact and precipitation in the open pore spaces at the grain edges. This certainly means that the dependence of S on the normal stress has changed which may be because the grains have grown in time via pressure solution. Nevertheless, S started to decrease and therefore Z* decreased. The solute diffusion coefficient, D may also have changed over time from first increasing to later decreasing, although why D would change like this is unclear.

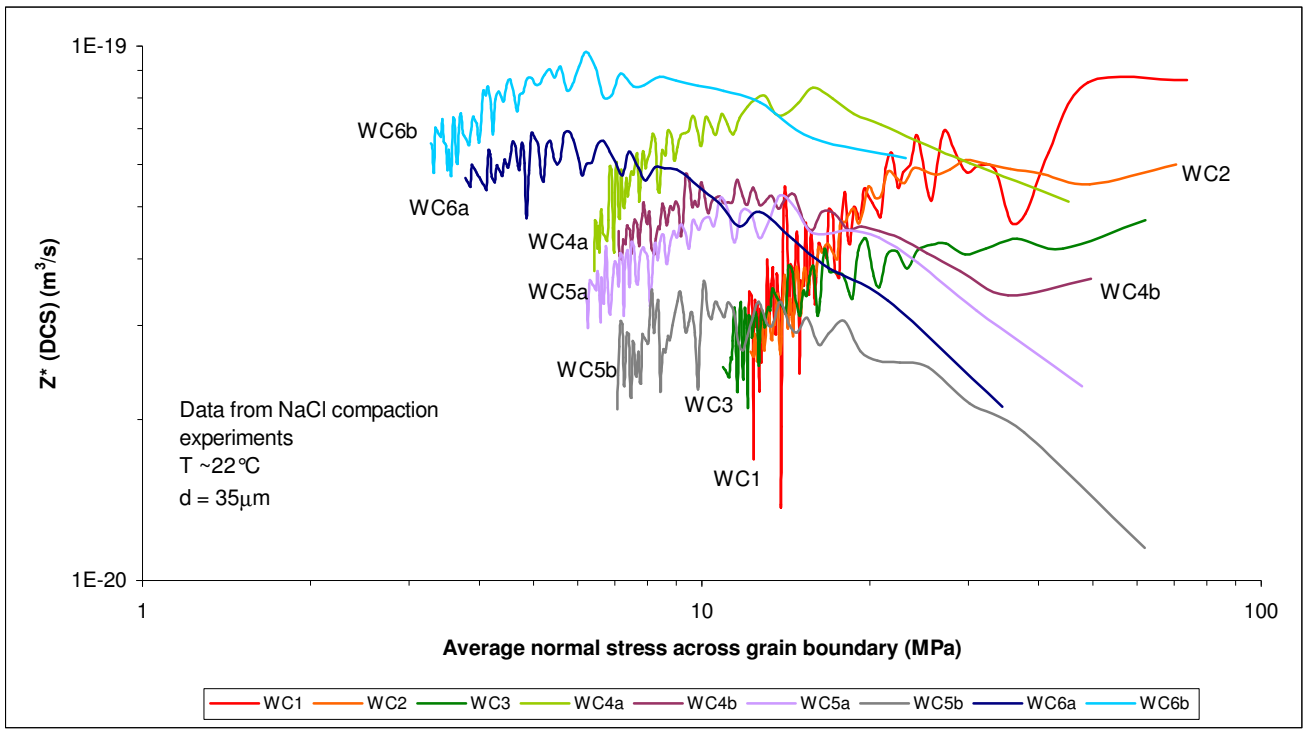

Figure 18 A Log-log plot of the diffusivity Z* versus the average normal stress across the grain boundary for the compaction experiments. This plot only displays the data with grain size of 35 micron

Figure 18 is the same diagram but shown with lines instead of points and the data from experiments with a greater grain size of 35 micron were left out to clarify the processes that occur in relationship with the average normal stress and the diffusivity, Z*. All the data lies within 1 order of magnitude from 1E-20 m^3/s until 1E-19 m^3/s. It is apparent that data from the first three experiments with a relatively larger applied stress show a different trend than the other experiments.

In Figure 19 and Figure 20 these have been separated in order to see the difference more clearly. What is apparent is that for Figure 19 that the greater the applied stress, on average, the higher the diffusivity. I.e. more weights on the salt column mean a faster diffusion in the grain boundaries. Also the figure displays a positive correlation between the average normal stress on the grain boundaries and the diffusivity which is gradually moving towards a plateau. This means that at a certain moment the

diffusion in the grain boundaries becomes independent of the normal stress. Figure 20, on the other hand, shows a completely different picture. The diffusivity is still within 1E-20 m^3/s and 1E-19 m^3/s, but for all experiments there is initially a positive correlation suddenly changing to a negative correlation between the average normal stress on the grain boundaries and the diffusivity. The change-over occurs around 10 MPa, as can be seen. This must mean that other processes occur in a higher stress regime such as "plastically-coupled pressure solution accompanied by microcracking and fluid assisted recrystallisation" [Spiers and Brzesowsky, 1993]. In addition, the position of each curve does not follow logically. Data with the highest diffusivity is WC6b, the experiment with the lowest applied stress. This is followed by WC6a, but that curve quickly decreases rapidly to a lower diffusivity. However, the next curve below is WC4a followed by WC4b, WC5a and lastly WC5b. The experiments WC4a and b have a higher applied stress than WC5a and b. This compares with Figure 19, where the higher the applied stress, the higher the diffusivity. Bear in mind that in Figure 19 the diffusivity is initially still around WC5b but at a higher normal stress. Lastly, it is apparent that initially a lot of fluctuations can be seen in each curve, but that the "tail" of each curve is smooth and has a negative slope except for WC4b. Nevertheless, the fact that a negative correlation follows a positive correlation means that something is going on in the grain boundary. Note that the grain size used in these experiments was relatively small (35 microns). This means that other forces, such as surface tension could be playing a role in either the increasing grain boundary fluid thickness followed by a steady decreasing grain boundary fluid thickness, or by a change in the solute diffusion coefficient, D. If the latter is true, then the processes at the grain boundary would indeed be very difficult to explain. Also note that experiments WC8 and WC9 do not show this change-over, but only a negative correlation. In those experiments a greater grain size was used (see Figure 17).

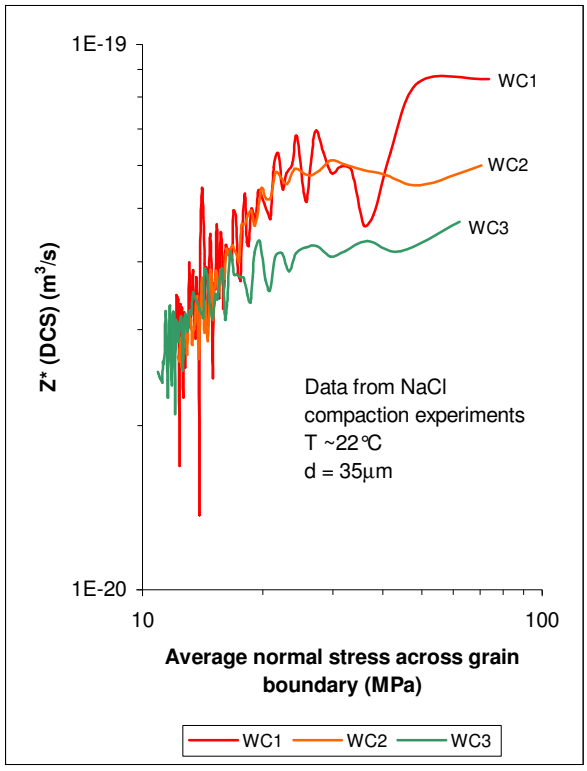

Figure 19 A Log-log plot of the diffusivity Z* versus the average normal stress across the grain boundary. This time only the first 3 experiments are shown as they deviate from the others.

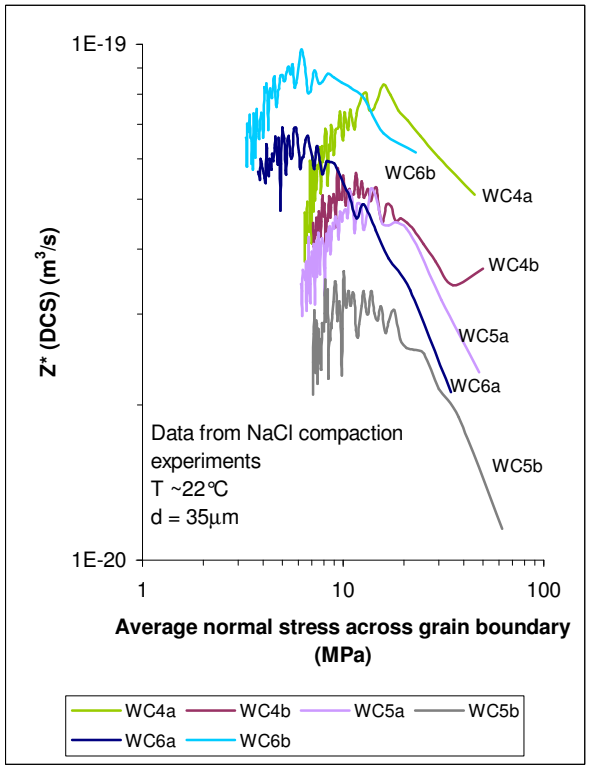

Figure 20 A Log-log plot of the diffusivity Z* versus the average normal stress across the grain boundary. Here the rest of the experiments are shown.

The following two figures, Figure 21 and Figure 22, demonstrate how the applied stress, σ_e does depend on Z*. The large scatter of data is due to the variation of volumetric strain and strain rate in each experiment. In the latter figure, Z* has been slightly changed in that the constant A is taken out of the formula (see Eqn. 1.17) as well as the applied stress. Z* is then denoted as E. The near one-on-one relationship of log(E) versus log(σ_e) is the result. This means that Z*, the diffusivity does depend on the applied stress but not by a great amount because the slope is fairly close to 1.

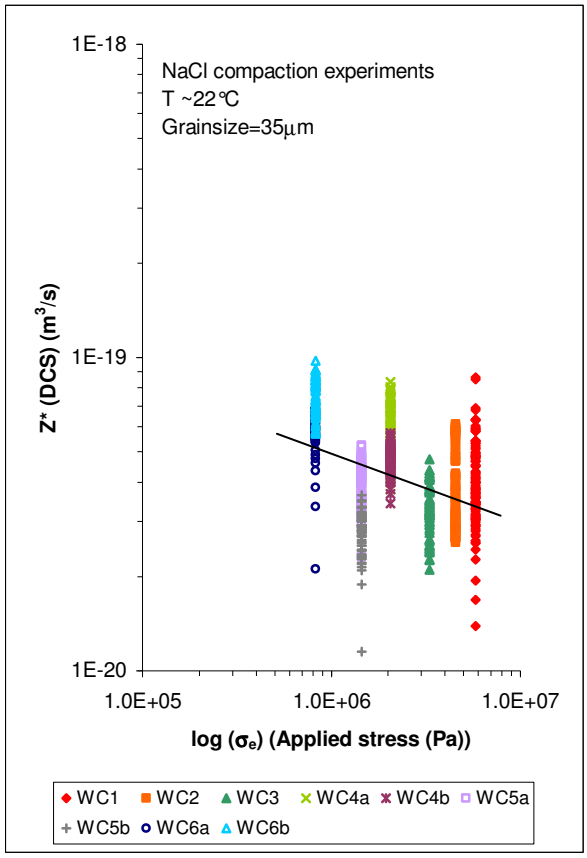

Figure 21 Log-log plot showing the relationship between the diffusivity, Z* and the applied stress for the compaction experiments

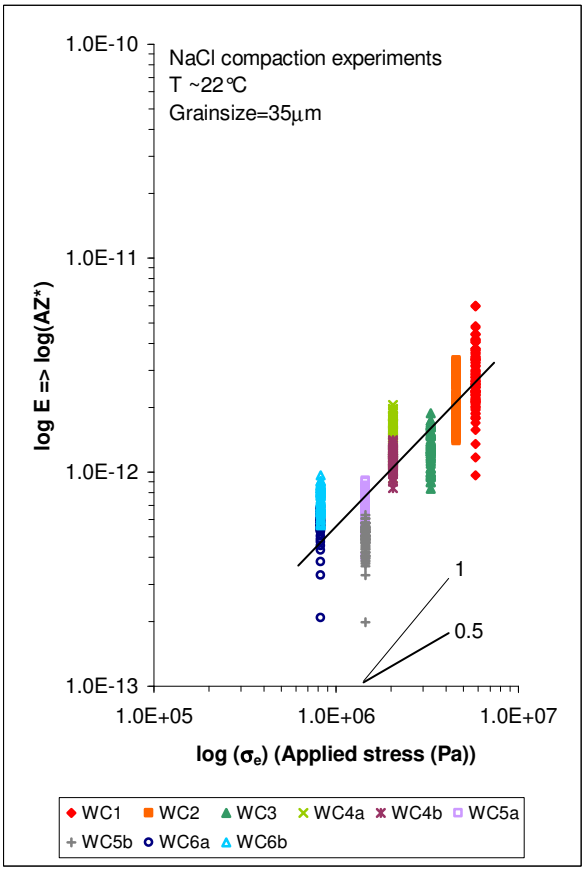

Figure 22 Log-log plot of the diffusivity multiplied by an "unknown" constant, A (previously taken as '18') versus the applied stress

5.2. Electrical conductivity experiments

5.2.1. Optical observations

As mentioned before, notice that in Figure 8(d) a second ring has formed, three quarters around the cone. After careful examination of an animation of the micrographs, it was clear that a thin film of salt was forming on the crystal surface. The dark lines visible in Figure 9 probably represent the front edge of that film of precipitated salt. The extra salt cannot have come from the NaCl-glass boundary, there is simply too much mass deposited on the crystal surface and cannot account for the removal at the cone/crystal contact. It cannot have come from the outer edges of the crystal either because there is simply no driving force for dissolution and precipitation to occur at that contact. The salt most likely comes from the brine solution as evaporation took place. The cell was apparently not sealed well enough. As soon as the precipitated salt came into contact with the NaCl -glass boundary, there may have taken place some undesired effects. For example the addition of extra material into the grain boundary may have caused it to widen (see Figure 8). As a result, S (fluid film grain boundary thickness) increased and thus the diffusivity, Z* increased. This can be seen in the results in the figures where Z* is plotted on the y-axis. The diffusivity increased by 2 – 3 orders of magnitude for the last 5 data points (see e.g. Figure 13 Log-linear plot of the logarithmic diffusivity, Z* versus the grain contact width, w. According to de Meer et al. [de Meer et al., 2002], local transport of NaCl is driven by "anisotropic surface energy" which is held responsible for the roughening of the surface as the surface strives to minimise its surface energy though the formation of crystal ledges by short range diffusion. This is clearly seen in the micrographs, in Figure 9. Especially at the end of day 11 the result of the building inwards of crystal ledges is seen at the NaCl-glass contact where the contact width has suddenly significantly increased (cf. second ring). The overgrowths as seen in Figure 8 are probably due to the precipitation of NaCl that comes from dissolution at the NaCl-glass contact. Furthermore, the rings seen in Figure 9 are due to the way the incision in the salt crystal was created. The conical surface was simply not smoothened enough for this effect to disappear.
Lastly, Figure 10, a micrograph taken at day 2 shows the three pathways where possibly some sort of brine solution flowed outwards and due to evaporation, salt precipitated along the way.

5.2.2. Resistance data

Figure 11 illustrates how, for a long time of about three and a half days, no resistance is measured across the contact at all. Then finally some resistance starts to build up in the NaCl-glass contact but soon afterwards somehow the contact must have opened again. At last the large peak in Figure 11 demonstrates how the NaCl-glass contact became closed and resistance was build up to a maximum of 628 kOhm. However, soon afterwards the peak dropped again down to a contact resistance of 80 – 70 kOhm. One may infer that the contact was at first still wetted and although the photos indicate the ring was already forming, meaning pressure solution was happening, there may have been some pathways in the NaCl contact where the brine solution in the lower compartment may have managed to go through to the upper compartment. This could be the case as shown in Figure 10. This then explains why no large resistance was recorded at first. At last due to increasing pressure solution at the contact, the large peak formed as the contact closed. The peak and the continuous further decreasing in resistance could either be due to the effect of competition between the increasing contact width, w and the decreasing normal stress, σ_n. Furthermore, from the images it is inferred that the effect of the formation of a new crystal surface on the original one started already before the large peak, but not before the smaller peak. However as long as the

precipitation of material on the NaCl surface and the growth of this new surface did not reach the ring forming in the centre, the experiment should have remained unaffected. The contact resistance does not seem to be dependent on w/r as seen in Figure 12, which is expected from Eq. 2 assuming S and D are constant. In fact, there seems to be no relationship at all.

From the experiment, there clearly is a near linear relationship between the diffusivity, Z* and contact width and an inversely proportional relationship of Z* and the normal stress, σ_n. However, Z* can be simplified to D, S, and C. It is unclear to which of these three factors increases or decreases the most with increasing contact width and increasing normal stress on the contact respectively. It could be caused by changes of the grain boundary fluid thickness (S) and diffusivity with σ_n, by a combined change for all three variables, or by a change in the grain contact structure, such as channels and islands formation. Perhaps in relation to the compaction experiments, more can be said about these three factors.

5.3. Comparison to NaCl compaction experiments

The following figure, Figure 23, compares the compaction data with the results from the electrical conductivity experiment.

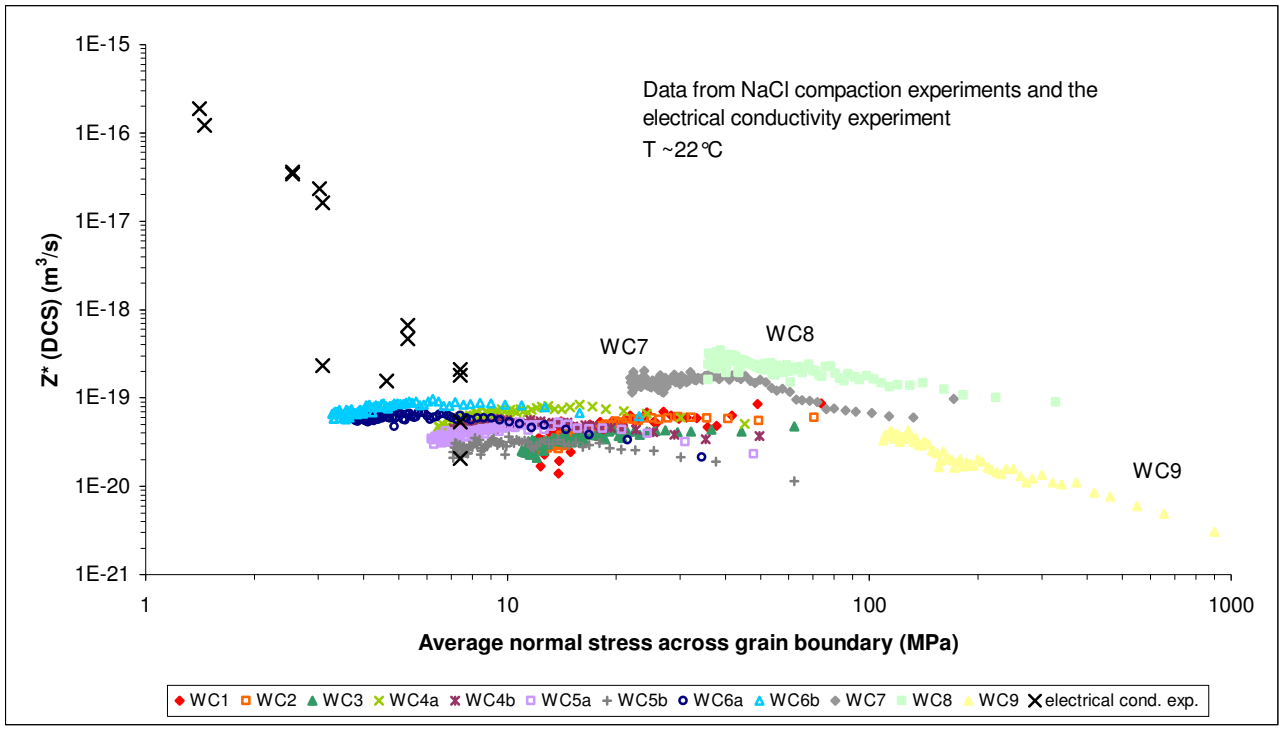

Figure 23 A Log-log plot of the diffusivity Z* versus the average normal stress across the grain boundary for the compaction experiments showing also the results from the electrical conductivity experiment

Figure 23 is the same plot as in Figure 17 except that this time the results from the electrical conductivity experiment were added. The data from the compaction experiments does give one the impression that the average normal stress is quite independent from the diffusivity in the grain boundaries except for WC9 where a grain size was used of 160 ± 15 micron. This is because most data shows far smaller variation than the data from the electrical conductivity experiment. At any rate, the grain size is important and strongly affects the diffusion of Na^+ and Cl^- ions in the grain boundary (or the diffusivity, Z*). In addition, diffusion has already been proven to be the rate limiting factor in pressure solution (see

section Va). Still the contrast in slopes is surprising between the two major experiments. The data from the electrical conductivity experiment follow a far steeper curve and is negative. The diffusivity values from the compaction experiments lie roughly in the same range between 3E-21 m^3/s and 4E-19 m^3/s, a bit lower. The points for the electrical conductivity that lie between 1E-17 m^3/s and 2E-16 m^3/s are surprisingly higher. Why this is, is unclear. It may have to do with the noticeable evaporation of the brine solution and the formation of a new salt layer on top of the crystal. At any rate, it is certain that S, the grain boundary thickness increased. This could have happened by excess precipitation in the grain contact due to the increasing rate of evaporation of water from the brine solution. This caused a counter force on the NaCl-glass contact and may have exceeded 2 N. The springs only need to contract ever so slightly and the NaCl-glass contact has increased in width by an unknown amount allowing the resistivity in the contact to suddenly drop to a range of 1E-17 m^3/s to 2E-16 m^3/s.

The differences between the electrical and the compaction experiments are important, though, to investigate. For example, the whole compaction process for the compaction experiments did occur within 25 minutes instead of 11 days for the electrical conductivity experiment although it is likely this has no effect on the result. Also the data from the electrical conductivity experiment did not involve separate NaCl grains and the contact was different as well. For the compaction experiments the contact was NaCl-NaCl type contact as for the electrical conductivity experiment the contact was an NaCl-glass contact. Therefore diffusion of salt through grain boundaries under pressure solution clearly depends on many factors. Unfortunately, the compaction experiments do not tell much more about the nature of Z*, and whether S, D, or C is the greater changing factor. However, as discussed in section 1 of the discussion, the sudden change in Z* versus the average normal stress does signify something. It is also apparent that when the grain size is larger than 35 micron but especially when it is around 150 ± 16 to 160 ± 15 micron, the relationship has completely become inversely proportional. That means that at 35 micron other processes play an important role, such as surface forces and that perhaps S does increase with increasing normal stress on the grain boundaries under these certain circumstances.

5.4. Comparison with previous work

5.4.1. Compaction experiments and electrical conductivity experiments

The slopes of the graphs from the present compaction experiments show the relationship of the strain rate, $\dot{\varepsilon}$ upon applied stress, σ_e, grain size, d, and the volumetric strain, e_v very well and compares well with previous studies too. The mechanical data fit the power law in the form: $\dot{\varepsilon} \approx e_v^{-q} \cdot \sigma_e^n \cdot d^{-p}$ where $q \approx 2$, n is slightly higher than 1, and $p = 3$. According to the theory these results strongly suggest pressure solution that is diffusion controlled.

Spiers and co-workers [Spiers and Brzesowsky, 1993] got very much the same results but with some more variation in the slopes; $p \approx 2-3$, $q \approx 2-3$, and $n \approx 1-4$. They used a greater range in stress though (from 1.1 – 8 MPa) and a greater grain size for the NaCl samples (98 – 410 μm). They demonstrate that at stresses lower than 4 MPa, tests relate very well to the theory, but at stresses higher than 4 MPa, 'in the upper stress regime,' a change in mechanical behaviour is observed. This can also be seen in Figure 19 and Figure 20 for the change in values for the diffusivity, Z*. The curves for experiments WC1, 2, 3 at stresses from about 3.32 MPa to 5.81 MPa are distinctly different from the curves obtained for lower stresses. Therefore, this phenomenon agrees quite well even at a grain size of $35 \pm 5 \mu m$, compared to the grain size Spiers et al. used which was $275 \pm 25 \mu m$. However, compared to the graphs showing the relationship of the strain rate, $\dot{\varepsilon}$ upon applied stress, σ_e, grain size, d, and the

volumetric strain, e_v, this distinction of a 'lower stress regime' and a 'higher stress regime' is not evident. Only in Figure 3 can we see that for a grain size of 160 ± 15 micron, the curve lies in a different orientation but may well have the same slope as the other curves, only at a lower strain rate.

den Brok and co-workers [den Brok et al., 1999] got for the relationship between the strain rate, $\dot{\varepsilon}$ upon applied stress, σ_e, grain size, d, and the volumetric strain, e_v, quite the same results; $q = 2-4$, $n = 1.6 \pm 0.5$, and $p = 2.8 \pm 0.5$. Only that their n value is somewhat higher than in the present experiments.

Continuing on, the Z* values of these compaction experiments all lie in a range of (4E-19 to 3E-21) m^3/s with V_m (molar volume) = 2.378E-5 m^3/mol and A = 12. Spiers and co-workers [Spiers and Brzesowsky, 1993] got values for Z* ranging from (2.59 + 0.94,-0.71)E-19 m^3/s with V_m = 2.693E-5 m^3/mol and A = 12. Both lie in the same range. Other studies share the same Z* values such as Schutjens and Spiers [Schutjens and Spiers, 1999] in a NaCl-NaCl crystal contact diffusion experiment. They obtained values for the "kinetic coefficient", Z* in the range of 4.6E-20 m^3/s to 4.6E-19 m^3/s with "most values clustering at the lower end." They obtained contact stresses of 1-7.5 MPa. Hickman and Evans [Hickman and Evans, 1992 , Hickman and Evans, 1991 , Hickman and Evans, 1995] also obtained Z* values: 3.7E-20 m^3/s to 1.8E-19 m^3/s, at contact stresses of 0.5-12MPa. The data was recalculated because they did their experiment at 50°C (see [de Meer et al., 2002]). They carried out crystal NaCl-NaCl and glass-NaCl experiments, but these values come from the latter experiment. In the former experiment they witnessed 'neck growth' at the grain contacts instead of pressure solution. Quite recently another experiment was carried out by de Meer and co-workers [de Meer et al., 2002] to verify if the diffusivity, Z* also is in the same range when measuring pressure solution at a NaCl-glass contact by electrical resistivity in the contact. The results are shown in Figure 15 and Figure 16. The data does indeed fall in the same range as this and previous experiments have shown, 2E-20 m^3/s < Z* = DSC < 2E-18 m^3/s to be exact with contact stresses of 1.1 – 10.1 MPa. Some Z* values from the compaction experiment are lower, down to 2E-21 m^3/s, but experience also much higher averaged normal stresses as seen in Figure 24.

The results from the present electrical conductivity experiment also show that 8 points do lie in the same region for the diffusivity coefficient. However, 5 values lie remarkably higher at Z* = 1E-17 m^3/s to 2E-16 m^3/s. The reason for this discrepancy has been discussed in section V, c. The electrical conductivity experiments and the results from Hickman and Evans and WC8 and WC9 all show an inverse dependence of Z* on the 'average' normal stress. Hickmann and Evans [Hickman and Evans, 1995] believed that this is caused by the effect of the normal stress on equilibrium film thickness as determined by surface forces. In addition, de Meer et al. [de Meer et al., 2002] argue that their results lie about an order of magnitude higher than the results from Hickman and Evans due to crystallographically controlled, periodic variations in grain boundary roughness, mean fluid thickness, and/or fluid film structure/diffusivity around the circular contact, yielding a (high) composite value for Z." Surface roughness certainly plays a role such as kink sites on the [001] crystallographic surface. For the granular pressure solution experiments there is no doubt that there are impurities as well on the surface of the salt grains that may influence pressure solution to some degree. It is also interesting to see that for the compaction experiments much higher stresses are obtained (due to smaller contact area between the grains) and, depending on the grain size, the relationship with Z is very similar (see Figure 24).

Note that the compaction experiments were carried out at room temperature (~22°C), but that the electrical conductivity experiments were carried out several degrees higher at ~26-28°C. It is unknown how much this difference in temperature contributes to the change in diffusivity in the grain boundary.

Overall the Z* values compare very well in the present experiments as well as with previous experiments. Unfortunately, the structure of the grain contact could not be examined for the electrical

experiment and for the compaction experiments time was short. However, in previous work by Spiers et al. [Spiers and Brzesowsky, 1993] there are micrographs of the microstructure of wet compacted salt samples taken. The micrographs of the lower stress regime clearly show indentations and overgrowths, typical for pressure solution. Little evidence of micro-cracking is observed, there is some contact cataclasis present though. Calculating separate values for S, D, and C was not attempted and may prove to be very difficult indeed. There is evidence though that S, the grain boundary width is responsible for any fluctuations and changes in the pattern of the data from the compression experiments and the electrical conductivity experiments. Lastly, the values for the slopes of the various relationships of the strain rate, $\dot{\varepsilon}$ upon applied stress, σ_e, grain size, d, and the volumetric strain, e_v are very good and also compare well with previous studies.

As a note to de Meer et al. [de Meer et al., 2002], they considered that the inverse dependence of Z* on the average normal stress "may be a property of wetted halite-glass contacts only." This has been proven to be false as seen in Figure 24.

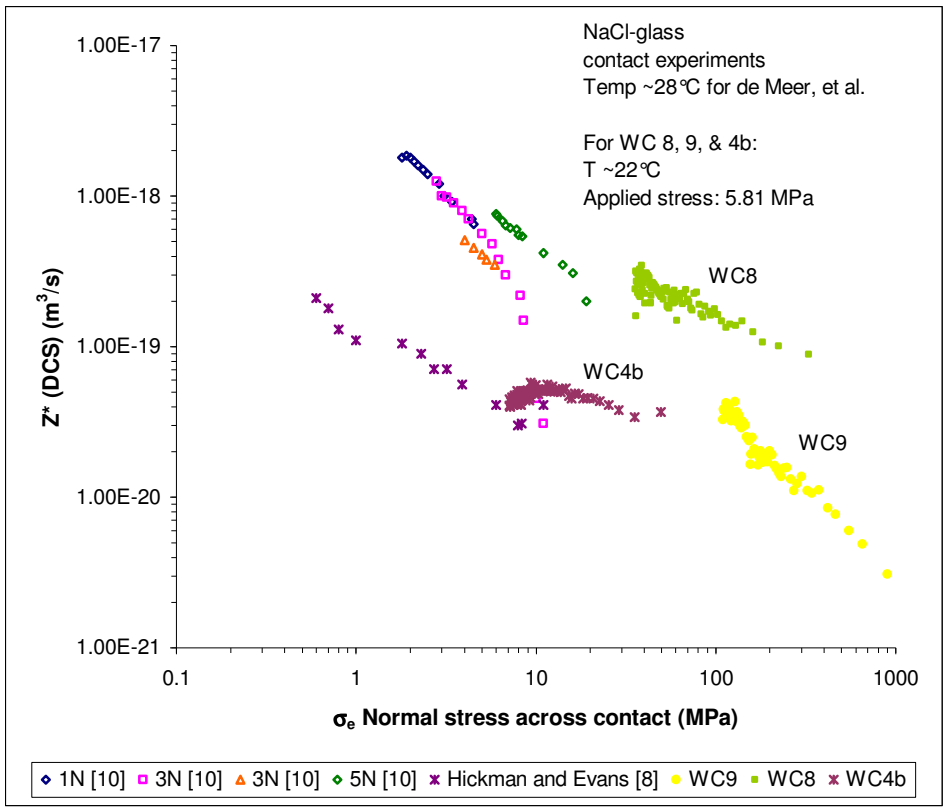

Figure 24 Log-log plot of the diffusivity, Z* versus the normal stress across the NaCl-glass contact. This graph shows surprisingly that WC8 and WC9 compare very well with the data from the electrical conductivity experiments done by de Meer et al. and Hickman and Evans.

Figure 24 shows that WC 8 and 9 compaction experiments with grain size of 150 ± 16 and 160 ± 15 micron respectively, compare very well with the data from the electrical conductivity experiments of de Meer et al. and Hickman and Evans, in fact more with the former authors because especially WC 9 lies with the same slope in the same direction as the 5 N / 3 N (orange triangles) experiments. I.e. the change in diffusivity with time and normal stress is the same. The inverse relation of Z* with the average normal stress for the compaction experiments is therefore possible (see also Figure 20). However for WC 9, and maybe WC 8 as well, the normal stress is far too big to be still accounted for pressure solution because

plastic deformation and fracture will occur at much lower values. Still these findings are indeed worth investigating in future work on pressure solution in salt. WC4b was plotted to show where the other compaction data would lie.

6. Conclusions

In the experiments presented here, compaction of granular salt under room PT conditions most likely occurred via plastic deformation first, reducing the porosity, and then when the brine solution was added compaction continued to occur but via pressure solution. Loading the annular NaCl-glass contact in the electrical conductivity experiment also probably caused some plastic deformation to occur initially, but was soon replaced by pressure solution and the dissolution of contact points followed by a steady growth of the contact by precipitation (see Figure 8, Figure 9, and Figure 10).

The compaction experiments produced the following results in agreement with the micromechanical theory; $\dot{\varepsilon} \approx e_v^{-q} \cdot \sigma_e^n \cdot d^{-p}$ where $q \approx 2$, n is slightly higher than 1, and $p = 3$ which proves that pressure solution in salt is diffusion dependent. For the calculation of the diffusivity, Z*, results show that it lies in the same range as results show from previous experiments namely between 3E-21 m^3/s to 4E-19 m^3/s.

For the electrical conductivity experiment, the magnitude of Z* = DCS after continuous contact formation is in the range of 2E-20 m^3/s to 2E-16 m^3/s. The eight data points at the lower end correlate well with previous experiments, but the 5 data points at the upper end suggest another process started to influence the resistivity in the NaCl-glass boundary (see section V, c). An inverse stress dependence on Z* is found also discovered by de Meer et al. [de Meer et al., 2002] and Hickman and Evans [Hickman and Evans, 1995] as well as for two compaction experiments WC8 and WC 9.

Thus the results suggest that the diffusivity, Z* can indeed be inversely related to the average normal stress for the compaction experiments but only under certain circumstances. For instance, the grain size must be relatively large, but not so large that plastic deformation starts to play a role. Also it seems that the average normal stress needs to be sufficiently large as well (see Figure 20) and that the applied stress may not be very large or the relationship between Z* and $<\sigma_n>$ remains still proportional (see Figure 19), hence the strong dependence on grain size.

D, C, and S could not be evaluated independently unfortunately, but the experiments suggest that S, the grain boundary fluid thickness plays an important role. The internal structure of the actively dissolving contact for the electrical conductivity experiment could not be investigated due to the way the experiment was set up. No further microscopic investigation was made on the compacted salt samples either.

7. References

C.J. Spiers, R.H. Brzesowsky, Densification behaviour of wet granular salt: theory versus experiment, in: Seventh Symp. On Salt, Vol. I, 1993, pp. 83-92.

S.H. Hickman, B. Evans, Growth of grain contacts in halite by solution transfer : implication for diagenesis, lithification, and strength recovery, in: B. Evans, T.-W. Wong (Eds.), Fault Mechanics and Transport Properties of Rocks, Academic Press, San Diego, CA, 1992, pp. 253-280.

S.H. Hickman, R. Sibson, R. Bruhn, Introduction to special section: mechanical involvement of fluids in faulting, J. Geophys. Res. 100 (1995) 12831-12840.

B. Bos, C.J. Spiers, Effect of clays on fluid-assisted healing behaviour of gouge-bearing faults, Earth Planet. Sci. Lett. 184 (2000) 199-210.

B. Bos, C.J. Peach, C.J. Spiers, Slip behavior of simulated gouge-bearing faults under conditions favoring pressure solution, J. Geophys. Res. 105 (2000) 16699-16717.

C.J. Spiers, P.M.T.M. Schutjens, R.H. Brzesowsky, C.J. Peach, J.L. Liezenberg, H.J. Zwart, Experimental determination of constitutive parameters governing creep of rocksalt by pressure solution, in: R.J. Knipe, E.H. Rutter (Eds.), Deformation Mechanisms, Rheology and Tectonics, Geol. Soc. London Spec. Publ. 54 (1990) 215-227.

S.H. Hickman, B. Evans, Experimental pressure solution in halite: the effect of grain/interphase structure, J. Geol. Soc. London 148 (1991) 549-560.

S.H. Hickman, B. Evans, Kinetics of pressure solution at halite-silica interfaces and intergranular clay films, J. Geophys. Res. 100 (1995) 13113-13132.

P.M.T.M. Schutjens, C.J. Spiers, Intergranular pressure solution in NaCl: grain-to-grain contact experiments under the optical microscope, Oil Gas Sci. Tech. Rev. IFP54 (1999) 729-750.

S. de Meer, C. J. Spiers, C. J. Peach, T. Watanabe, Diffusive properties of fluid-filled grain boundaries measured electrically during active pressure solution, Earth Planet. Sci. Lett. 200 (2002) 147-157.

X. Yang, Mathematical modeling of compaction and diagenesis in sedimentary basins, Thesis, submitted to the University of Oxford, 1997.

B. Martin, K. Röller, B. Stöckert, Low-stress pressure solution experiments on halite single crystals, Tectonphysics. 308 (1999) 299-310.

B. den Brok, M. Zahid, C. W. Passchier, Pressure solution compaction of sodium chlorate and implications for pressure solution in NaCl, Tectonophysics. 307 (1999) 297-312.

N.H. Sleep, M.L. Blanpied, Creep, compaction and the weak rheology of major faults, Nature 359 (1992) 687-692.

S. de Meer, C.J. Spiers, Creep of wet gypsum aggregates under hydrostatic loading conditions, Tectonophysics 245 (1995) 171-184.

Tada and Siever Geochim. Cosmochim. Acta, 50, 29 (1985)

den Brok and Spiers, J. Geol. Soc. London, 148, 541 (1991)

De Meer, S., Spiers, C.J., 1997. Uniaxial compaction creep of wet gypsum aggregates. J. Geophys. Res. 102, 875–891.

E.H. Rutter, Pressure solution in nature, theory and experiment, J. Geol. Soc. London 140 (1983) 725^740.

F. Renard, P. Ortoleva, J.P. Gratier, Pressure solution in sandstones: influence of clays and dependence on temperature and stress, Tectonophysics 280 (1997) 257-266.

8. Table of figures